

# Deep brain stimulation alleviates Parkinsonian motor deficits through desynchronizing GABA release in mice

Received: 20 September 2024

Accepted: 11 April 2025

Published online: 19 April 2025

Zongyi Xu<sup>1</sup>, Wei Duan<sup>1</sup>, Shuyu Yuan<sup>1</sup>, Xiaoxue Zhang<sup>1</sup>, Chong You<sup>2</sup>, Jin-Tai Yu<sup>1</sup>, Jian Wang<sup>1</sup>, Jia-Da Li<sup>3</sup>, Suixin Deng<sup>3</sup>✉ & Yousheng Shu<sup>1</sup>✉

High-frequency deep brain stimulation (DBS) at subthalamic nucleus (STN) is an effective therapy for Parkinson's disease (PD), but the underlying mechanisms remain unclear. Here we find an important role of asynchronous release (AR) of GABA induced by high-frequency stimulation (HFS) in alleviating motor functions of dopamine-depleted male mice. Electrophysiological recordings reveal that 130-Hz HFS causes an initial inhibition followed by desynchronization of STN neurons, largely attributable to pre-synaptic GABA release. Low-frequency stimulation at 20 Hz, however, produces much weaker AR and negligible effects on neuronal firing. Further optogenetic and cell-ablation experiments demonstrate that activation of parvalbumin axons, but not non-parvalbumin axons, from external globus pallidus (GPe) is both necessary and sufficient for DBS effects. Reducing AR diminishes the high-frequency DBS effect, while increasing AR allows low-frequency DBS to achieve a therapeutic benefit. Therefore, asynchronous GABA release from GPe PV neurons may contribute significantly to the therapeutic effects of high-frequency DBS.

Deep brain stimulation (DBS), an electrotherapeutic neuromodulation technique, has been utilized clinically for the treatment of movement disorders including Parkinson's disease (PD)<sup>1–4</sup>, essential tremor<sup>5,6</sup>, and dystonia<sup>7,8</sup>. This technique is also evolving and holds promise for the treatment of other neurological and psychiatric disorders, such as epilepsy<sup>9</sup> and major depression<sup>10,11</sup>. Subthalamic nucleus (STN) is a key circuit hub in the basal ganglia for the control of movement and one of the most common DBS targets for treating PD motor symptoms (e.g., bradykinesia, rigidity, and tremor)<sup>2</sup>. However, the underlying cellular and circuit mechanisms of the effect of STN DBS remains unclear and sometimes controversial, in terms of excitation or inhibition of subthalamic neurons in response to DBS. A better understanding of these mechanisms would help in

the selection of stimulation parameters in clinical practice, maximizing the beneficial effects while minimizing the adverse effects.

In comparison with early STN lesion experiments in MPTP-treated monkeys<sup>12</sup>, the relief of PD symptoms with high-frequency stimulation (HFS, >100 Hz) at STN is similar, suggesting that DBS at high frequencies would reduce the spiking activity of STN neurons and thus their output to the downstream brain regions<sup>13–15</sup>. However, the neural substrates affected by the DBS are complicated because the delivered electric pulses will non-specifically stimulate all tissues in the current pathways, including not only STN neurons but also traversing axons from other brain regions. These axons contain glutamatergic fibers (hyperdirect pathway) mainly from the motor cortex and GABAergic fibers from globus pallidus externa (GPe). Therefore, DBS can

<sup>1</sup>Department of Neurology, Huashan Hospital, Institute for Translational Brain Research, State Key Laboratory of Medical Neurobiology, MOE Frontiers Center for Brain Science, Innovative Center for New Drug Development of Immune Inflammatory Diseases, Ministry of Education, Fudan University, Shanghai, China.

<sup>2</sup>Shanghai Institute for Mathematics and Interdisciplinary Sciences, Fudan University, Shanghai, China. <sup>3</sup>Center for Medical Genetics, School of Life Sciences, MOE Key Laboratory of Rare Pediatric Diseases, Hunan Key Laboratory of Animal Models for Human Diseases, Central South University, Changsha, China.

✉ e-mail: [sxdeng@csu.edu.cn](mailto:sxdeng@csu.edu.cn); [yousheng@fudan.edu.cn](mailto:yousheng@fudan.edu.cn)

modulate the spiking activity of STN neurons and the sign (increase or decrease) of modulation depends on the net effect of direct neurite stimulation and evoked synaptic transmission (both excitatory and inhibitory), thus exerting modulatory effects on spiking activity of downstream neurons at globus pallidus interna (GPi) and other target brain regions. It is of interest to know how synaptic transmission and spiking activity of STN neurons respond to extracellular electric shocks at both low and high frequencies.

In response to HFS, but not low-frequency stimulation (LFS), certain types of synapses not only show synchronous release (SR) of neurotransmitter that is tightly coupled to individual presynaptic action potentials (APs), but also exhibit asynchronous release (AR)<sup>16,17</sup>. The synaptic AR events occur during and long (tens of milliseconds to a few seconds) after the HFS. Previous studies in neocortical slices demonstrate that AR of GABA from fast-spiking interneurons desynchronizes principal pyramidal neurons<sup>18</sup>, AR of glutamate from pyramidal neurons not only desynchronizes their own spiking activity via autapses<sup>19</sup> but also causes long-lasting and randomized discharges in postsynaptic cells<sup>16</sup>. Considering that an abnormal increase in beta oscillation is closely associated with PD motor symptoms, and HFS reduces rhythmic neural activity in the beta band<sup>20</sup>, we hypothesize that DBS at high frequencies may cause asynchronous neurotransmitter release and thus desynchronize spiking activity of STN neurons and pathological network activities, producing beneficial behavior outcomes.

We performed whole-cell recording in acute slices from dopamine-depleted (DD) mice and detected much more robust AR of both GABA and glutamate in response to HFS at 130 Hz, as compared to LFS at 20 Hz. HFS causes initial inhibition and later desynchronization of spiking activity of STN neurons, mainly due to GABAergic synaptic inputs from GPe parvalbumin (PV) neurons. Behavioral test of DD mice indicates that the activation of PV axons is both necessary and sufficient for the beneficial high-frequency DBS. Further experiments manipulating the AR strength suggest an important role of AR in alleviating Parkinsonian motor deficits. Therefore, high-frequency DBS desynchronizes GABA release from GPe PV neurons and thereby the spiking activity of STN neurons, leading to an improvement of motor functions.

## Results

### Asynchronous neurotransmitter release occurs during HFS at STN

We injected 6-hydroxydopamine (6-OHDA) into the medial forebrain bundle (MFB) bilaterally to cause dopamine depletion in mice (male, 8–12 weeks old). Indeed, immunostaining revealed a strong reduction of tyrosine hydroxylase (TH) signals on both sides of the striatum (Fig. 1a, b). Through the two electrodes implanted into bilateral sides of STN (see “Methods”), we delivered electric DBS (Supplementary Fig. 1a) and found that the HFS at 130 Hz (but not the LFS at 20 Hz) significantly increased the locomotion velocity (Fig. 1c, d) and decreased the percentage of immobility time (130 Hz, Pre  $73.21 \pm 5.35\%$  vs. Stim  $44.11 \pm 3.66\%$ ,  $n = 12$  mice, paired  $t$ -test, two-sided,  $P = 0.0009$ ) throughout the long-lasting stimulation, indicating a therapeutic effect of HFS in the bilateral DD mice.

Next, we performed whole-cell recording from STN neurons in sagittal slices of basal ganglia to examine synaptic responses to electric stimulation at high or low frequencies. We first examined the inhibitory postsynaptic current (IPSC) with a high- $\text{Cl}^-$  pipette solution and addition of 1.5 mM kynurenic acid (Kyn) in the bath to block fast glutamatergic transmission (Fig. 1e). With prolonged HFS (30 s in train duration) similar to clinical DBS treatment (Supplementary Fig. 1a), we detected IPSCs (Fig. 1f) tightly coupled to individual electric pulses, reflecting SR of presynaptic neurotransmitter vesicles. In addition, HFS also triggered barrages of synaptic events that are not tightly associated with individual pulses, indicating the occurrence of AR (Fig. 1f). These AR-related synaptic events also occur during LFS, but much less

than those during HFS. As shown in Fig. 1g, overlay of current traces evoked by individual electric pulses during the HFS reveals a progressive reduction in the amplitude of evoked IPSCs (i.e., SR events) but a progressive increase in the number of AR events. In contrast, the amplitude of evoked IPSCs remains similar across the entire LFS period. Bath application of 50  $\mu\text{M}$  picrotoxin (PTX) or bicuculline (BCC) blocked the evoked synaptic currents (Supplementary Fig. 1b–f), indicating that they were mediated by GABA<sub>A</sub> receptors. To calculate the total IPSC charge and estimate the contribution of SR and AR, we removed the stimulation artifacts and fitted each SR response with  $\alpha$ -synapse functions (Supplementary Fig. 1b–d, also see “Methods”). In comparison with LFS, HFS evoked much larger total charge and SR charge within the initial several seconds (Fig. 1h, i). The AR ratio and the basal current, a DC shift largely attributable to AR<sup>16,21</sup>, were significantly higher during the whole period of HFS than those of LFS (Fig. 1j, k), and the AR ratios for both HFS and LFS remained stable during the stimulation (Fig. 1j). Therefore, following the initial seconds of stimulation, the total charge induced by HFS and LFS was primarily mediated by AR and SR, respectively. Similar results were obtained from control mice (untreated C57 mice), where the total charge, SR charge, AR ratio, and basal current with HFS differed significantly from those with LFS (Supplementary Fig. 1g–k). Comparison of the IPSC AR ratio reveals a substantial decrease in DD mice with HFS, but not with LFS (Fig. 1l).

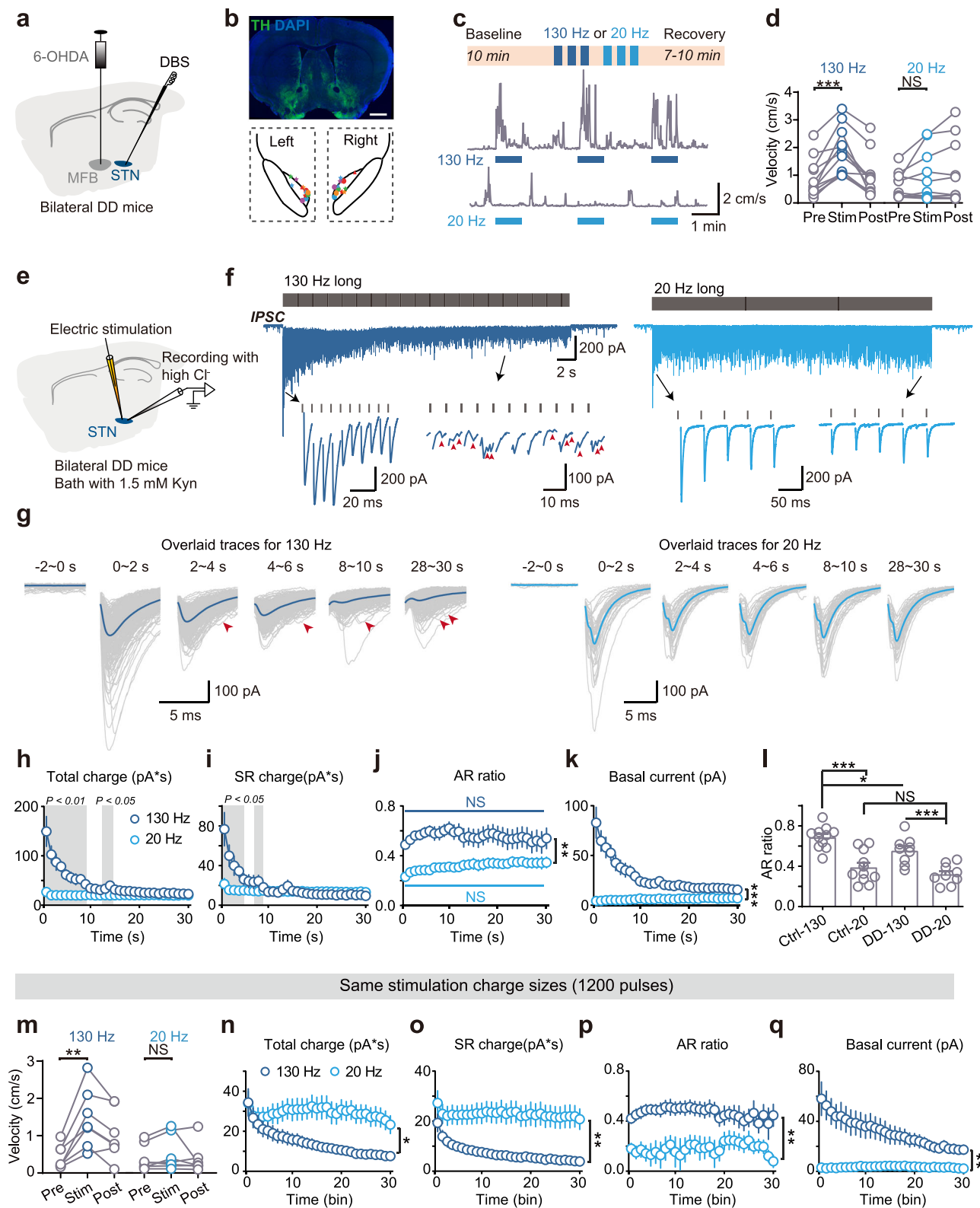
Considering that these distinct outcomes of HFS and LFS may result from differences in the charge size of electric stimulation, we then delivered stimulation with identical charge sizes, i.e., 1200 electric pulses for both HFS and LFS. Again, in animals with DBS, HFS (but not LFS) significantly increased the locomotion velocity (Fig. 1m). Although much larger total charge and SR charge were observed with LFS, HFS dramatically increased the AR ratio and basal current (Fig. 1n–q), suggesting that the therapeutic effect of DBS could be attributed to the strong AR associated with HFS rather than the number of stimulation pulses.

STN neurons also receive glutamatergic synaptic inputs. We next examined the evoked excitatory postsynaptic current (EPSC) (Supplementary Fig. 2a–f). Similar to IPSCs, the EPSC total charge within the initial several seconds with HFS was significantly greater than that of LFS, largely due to an increase in AR strength (Supplementary Fig. 2c–f). Different from IPSCs, the AR ratio showed no significant difference between control and DD mice (Supplementary Fig. 2g).

Together, these results show that the prolonged synaptic stimulation at STN produces both synchronous and asynchronous neurotransmitter release, with much stronger AR with HFS. Since the SR charge decreases significantly within the first 4 s of HFS and then stabilizes at low levels, AR becomes the dominant mode of synaptic transmission ~4 s after stimulation onset, coinciding with the persistence of DBS effect.

### GABAergic synaptic transmission plays a dominant role in DBS effect

Next, we examined spiking responses of STN neurons to synaptic stimulation in acute slices. Most of the recorded cells showed spontaneous firing with instantaneous frequency (1/ISI) coefficient of variation (CV) of ~0.2, and the firing rate and CV in DD mice were similar to those of control mice (Supplementary Fig. 2h–j). Since the differences between high and low frequencies in the IPSC recordings stabilize within several seconds (Fig. 1h–k), we employed a shorter train stimulation (10 s in duration) to examine the effects of HFS and LFS on spontaneous firing of STN neurons (Fig. 2a–c). The stimulation electrode was placed 100–150  $\mu\text{m}$  away from the recorded cell to avoid direct stimulation of its soma and neurites. During the 10-s HFS (130 Hz) in slices of DD mice, we observed an initial strong inhibition of the spontaneous firing, followed by a gradual recovery. In contrast, 20 Hz stimulation showed no significant effect (Fig. 2b–e). The CV of instantaneous frequency was significantly increased with HFS, but not



LFS (Fig. 2f), suggesting a pronounced desynchronization of spiking activity. Similar results were obtained in cell-attached recording mode (Supplementary Fig. 3).

Previous studies revealed lower concentrations of Ca<sup>2+</sup> and Mg<sup>2+</sup> under physiological conditions<sup>22</sup>. We therefore also examined the modes of synaptic transmission and neuronal firing in response to HFS and LFS at a more physiological level of Ca<sup>2+</sup> (1.2 mM) and Mg<sup>2+</sup> (1 mM) in the bath solution. We detected comparable strength of AR and

similar effect of electric stimulation on spiking activity of STN neurons (Supplementary Fig. 4), indicating that AR and desynchronized firing also occur under these more physiological conditions. These results suggest a dominant role of GABAergic transmission, particularly its SR mode, in mediating the initial inhibition induced by HFS. Moreover, the desynchronized spiking activity of STN neurons could be attributable to AR of neurotransmitters, including both glutamate and GABA, as suggested by previous findings in neocortical neurons<sup>16,18</sup>.

**Fig. 1 | HFS induces asynchronous release (AR) of neurotransmitter and alleviates movement deficit in DD mice.** **a** Schematic showing the injection of 6-OHDA into MFB to induce bilateral dopamine-depleted (DD) Parkinsonian mouse model, as well as bilateral DBS at the STN. **b** Top, a representative image ( $n = 6$  mice) showing the absence of TH immunosignals in the dorsal striatum. Scale bar, 1 mm. Bottom, symbols indicate the stimulation sites at the STN in experiments shown in **(d)**. **c** Representative behavior test showing increases in locomotion velocity in response to STN DBS at 130 Hz (high-frequency stimulation, HFS) but not at 20 Hz (low-frequency stimulation, LFS). **d** Group data comparing the average velocity within 60 s before, during, and after the DBS in DD mice ( $n = 12$  mice). 130 Hz Pre vs. Stim ( $P = 0.0005$ ), 20 Hz Pre vs. Stim ( $P = 0.4697$ ), Wilcoxon matched-pairs signed rank test, two-sided. **e** Schematic showing local electric stimulation and IPSC recording with high-Cl<sup>-</sup> pipette solution in STN slices of DD mice. **f** Representative current traces (with stimulation artifacts removed) of IPSCs evoked by long-lasting trains (30 s) of HFS or LFS. SR and AR events can be clearly identified in traces with HFS. Red arrowheads indicate AR events. Few AR events can be detected in traces with LFS. Insets, expanded traces for clarity. **g** Gray, overlaid current traces before the stimulation onset ( $-2$  to  $0$  s) and those evoked by individual electric pulses during indicated time periods of stimulation (2 s each). Blue, the average traces. Red arrowheads indicate AR events. **h–k** Group data showing

changes in the total charge, SR charge, AR ratio (AR charge to total charge), and basal current of the evoked IPSCs during the HFS and LFS (bin size, 1 s;  $n = 9$  neurons from 4 mice). Gray, time points with significant differences. Paired  $t$ -test or Wilcoxon matched-pairs signed rank test for **(h, i)** (two-sided): 130 vs. 20 Hz in **(h)**  $0–9$  s  $P < 0.01$ ,  $12–14$  s  $P < 0.05$ ; in **(i)**  $0–5$  and  $7–8$  s  $P < 0.05$ . For **j**, 130 vs. 20 Hz: two-way ANOVA without adjustments,  $P = 0.0022$ ; changes over time: 130 Hz ( $P > 0.9999$ ), 20 Hz ( $P = 0.9246$ ), one-way ANOVA without adjustments. For **(k)** 130 vs. 20 Hz ( $P = 0.0008$ ), two-way ANOVA without adjustments. **l** Group data comparing the AR ratio of IPSCs evoked by 130 and 20 Hz stimulation in control ( $n = 11$  neurons from 4 mice) and DD mice ( $n = 9$  neurons from 4 mice). DD: 130 vs. 20 Hz, paired  $t$ -test, two-sided,  $P = 0.0006$ ; Ctrl: 130 vs. 20 Hz, paired  $t$ -test, two-sided,  $P < 0.0001$ ; Ctrl vs. DD, 130 Hz:  $P = 0.0247$ , 20 Hz:  $P = 0.2706$ , unpaired  $t$ -test, two-sided. **m** Similar to **(d)** but with the same charge size of DBS (1200 pulses) in both HFS and LFS ( $n = 7$  mice). 130 Hz, Pre vs. Stim ( $P = 0.0032$ ), paired  $t$ -test, two-sided; 20 Hz, Pre vs. Stim ( $P = 0.1094$ ), Wilcoxon matched-pairs signed rank test, two-sided. **n–q** Similar to **(h–k)** but with the same stimulation charge size (bin size, 40 stimulation pulses;  $n = 10$  neurons from 4 mice). 130 vs. 20 Hz, two-way ANOVA without adjustments. **n**  $P = 0.0124$ ; **o**  $P = 0.0017$ ; **p**  $P = 0.0024$ ; **q**  $P = 0.0010$ . Data are represented as mean  $\pm$  SEM. NS not significant; \* $P < 0.05$ , \*\* $P < 0.01$ , \*\*\* $P < 0.001$ . Source data are provided as a Source Data file. See also Supplementary Figs. 1 and 4.

To further dissect the contribution of GABAergic and glutamatergic transmission to the therapeutic effect of DBS, we performed pharmacological experiments in DD mice (Fig. 2g–j). Similar to the behavioral results shown in Fig. 1a–d, we observed increases in locomotion velocity during the 130-Hz DBS, but not with 20-Hz. Bilateral injection of bicuculline (BCC, 500  $\mu$ M), a GABA<sub>A</sub> receptor antagonist, completely blocked the effect of 130-Hz DBS on the locomotion velocity (Fig. 2h, j) and the percentage of immobility time (Pre  $86.78 \pm 6.52\%$  vs. Stim  $82.89 \pm 5.77\%$ ,  $n = 5$  mice, paired  $t$ -test, two-sided,  $P = 0.3995$ ), while vehicle injection produced no change (Fig. 2h, i). In both experiments, 20-Hz DBS showed no obvious effect before and after the application of BCC or vehicle (Fig. 2i, j). Cell-attached recording in acute slices further demonstrated that BCC (50  $\mu$ M) abolished the effect of HFS on spontaneous firing of STN neurons (Supplementary Fig. 3). These results demonstrate a predominant role of GABAergic synaptic transmission in STN DBS, while the contribution of activating glutamatergic inputs appears relatively negligible. Thus, in the following experiments, we focus on GABAergic inputs of STN neurons.

### Activation of axons from GPe PV neurons is necessary and sufficient for STN DBS effect

Since GPe provides the majority of GABAergic synaptic inputs to STN<sup>23</sup>, we next examined its contribution to the DBS beneficial effects (Fig. 3, Supplementary Fig. 5 and 6). We first injected adeno-associated virus (AAV) in wild-type C57 mice to allow oChIEF expression in GPe neurons nonspecifically (Fig. 3a). We chose oChIEF because it allows GPe neurons to follow high-frequency light stimulation (Supplementary Fig. 5a–e). Bilateral optic stimulation of GPe axons (6 trials of 130 Hz or 130/20 Hz alternative stimulation, 1 ms in pulse duration, 30 s for each trial, 90-s interval) was delivered to the STN of the tested mice in a square open field. Optic HFS significantly increased the velocity of movement in DD mice (Fig. 3b,c). No effect was observed in mice with injections of control virus (tdTomato only) (Fig. 3c). Similar to electric DBS, 20-Hz light stimulation showed no effect on locomotion both in oChIEF and control mice (Supplementary Fig. 5f–h).

GPe neurons are mostly GABAergic and show high heterogeneity, including neurons expressing cell markers such as parvalbumin (PV), Lhx6, and Foxp2. Previous studies show that constant opto- or chemogenetic stimulation of PV neurons improved motor functions<sup>24,25</sup>. We next examined whether the activation of PV or non-PV axons from GPe in the STN exerts an effect on the locomotion of DD mice (Fig. 3d–k). We repeated the above experiments in PV-Cre mice with

injection of viruses allowing expression of oChIEF in Cre-positive neurons (Fig. 3d) and found that  $75.17 \pm 7.86\%$  ( $n = 25$  sections from 5 mice) of mCherry-positive cells contained PV immunosignals (Fig. 3j, k). Similar bilateral optic HFS (130 Hz) of GPe-PV axons in STN also significantly increased the locomotion velocity and decreased the percentage of immobility time (Fig. 3e, f and Supplementary Fig. 6) of DD mice, while no effect was observed in control mice with mCherry expression alone (Fig. 3e,f and Supplementary Movie 1). Again, LFS at 20 Hz produced no effect on locomotion (Supplementary Figs. 5i–k and 6a–f, Supplementary Movie 1). Considering that GPe PV neurons discharge at 10–40 Hz in DD mice<sup>25–27</sup>, we also examined the effect of a slightly higher frequency at 45 Hz (medium frequency stimulation, MFS). Optic MFS also offered marginal improvement of motor functions (Supplementary Fig. 6a–f). Close examination of the locomotion patterns (e.g., walking, grooming, tremoring, and rearing) revealed that HFS and MFS increased the percentage of time with walking, while LFS actually resulted in more tremoring (Supplementary Fig. 6f). We next expressed oChIEF in GPe non-PV neurons using a Cre-off virus (AAV-DO-oChIEF-mCherry) and repeated the above experiments (Fig. 3g). The majority ( $78.15 \pm 2.63\%$ ,  $n = 27$  sections from 6 mice) of the mCherry-positive cells showed no PV immunosignals, indicating a high specificity of this Cre-off strategy (Fig. 3j, k). Surprisingly, similar optic stimulation, with frequencies of both 130 and 20 Hz, produced no obvious change in locomotion velocity (Fig. 3h, i and Supplementary Fig. 5l, m).

To ascertain the necessity of activation of PV axons in the efficacy of STN DBS, we selectively ablated PV-positive cells in GPe by injecting a Cre-dependent virus that allows the expression of Caspase3 in PV-Cre mice (Fig. 3l). Immunostaining experiments 3–5 weeks after the virus injection showed a complete loss of PV-positive cells in GPe (Fig. 3m). In the open field test, mice with PV cell ablation exhibited a significant decline in spontaneous motor activity, as reflected by the reductions in the total mobile time, total travel distance, and mean velocity (Supplementary Fig. 5n, o). In the rotarod test, however, these mice showed intact motor ability and motor learning capability after PV cell ablation (Supplementary Fig. 5p). Next, we examined the effect of STN DBS in DD mice with GPe PV cells ablated (Fig. 3l–p) whose baseline locomotion velocity was similar to that of PV-Cre DD mice (Fig. 3n). Neither the HFS (130 Hz) or the LFS (20 Hz) showed any effect on movement (Fig. 3o and Supplementary Movie 2), as indicated by no significant change in the mean velocity during the 60-s stimulation (Fig. 3p).

Considering that electric or optic DBS may exert their effects through AP backpropagation along PV axons and thereby activation of other downstream nuclei of GPe, we next sought to examine the

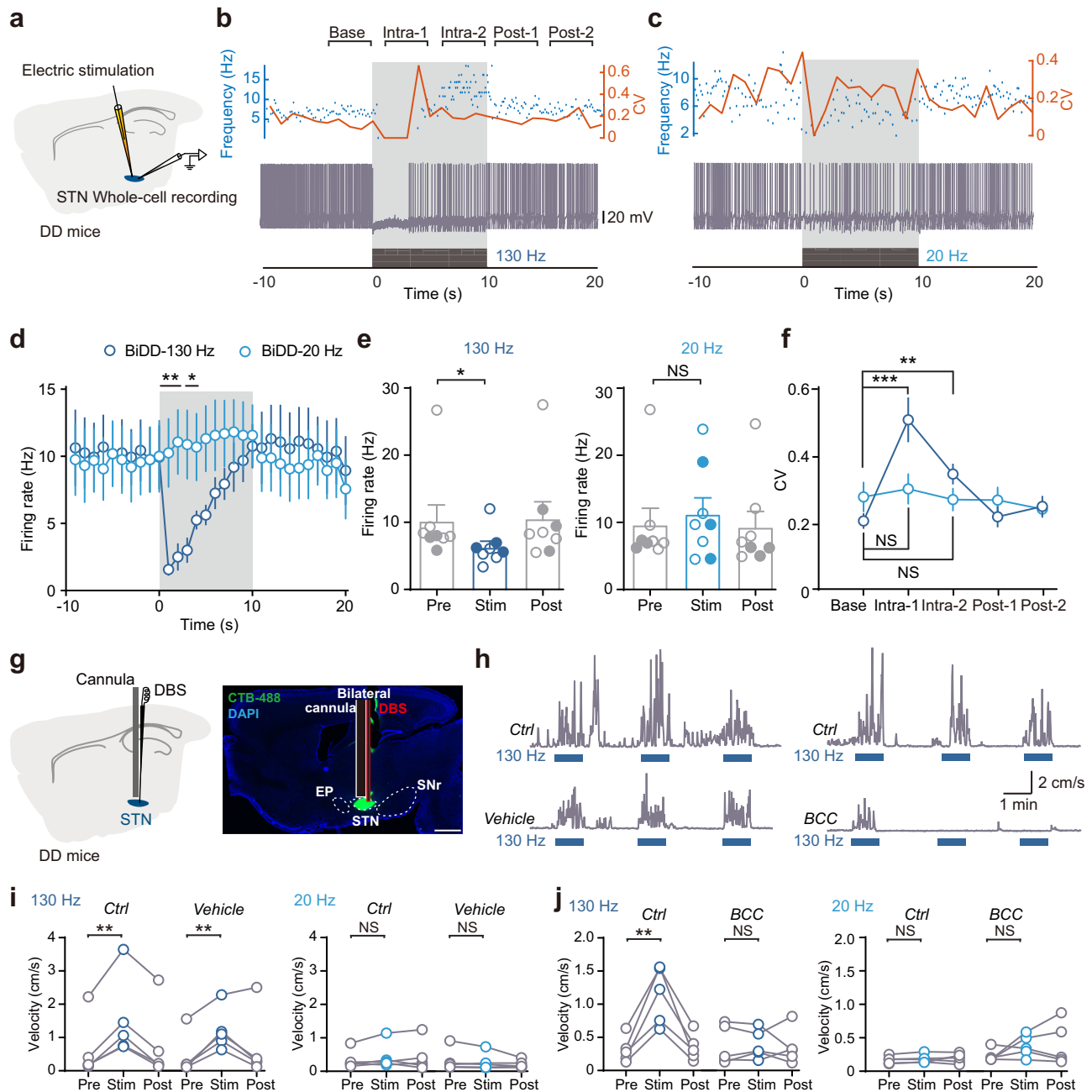
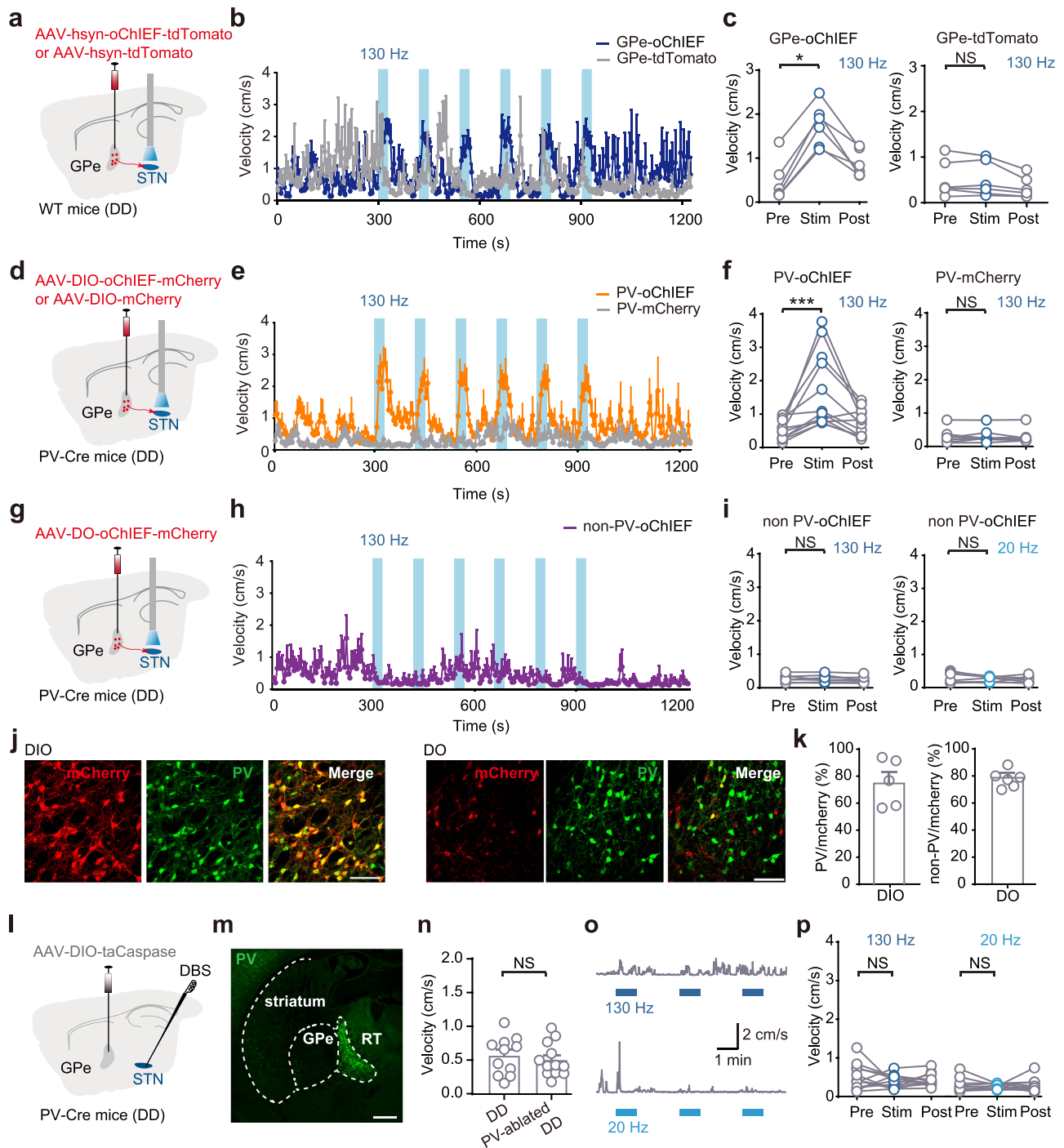


**Fig. 2 | GABAergic synaptic transmission plays a dominant role in DBS.**

**a** Schematic showing whole-cell recording (with normal pipette solution) with local electric stimulation in STN slices of DD mice. Middle and bottom, example current-clamp recording showing the effects of HFS (**b**) and LFS (**c**) on spontaneous firing of STN neurons. Top, plots of the instantaneous frequency of APs and its coefficient of variation (CV, bin size: 1 s). Time windows (4 s) before, during, and after the stimulation were shown for data analysis in (**f**). **d** Group data showing changes in the firing rates in response to HFS and LFS over time ( $n = 8$  neurons from 5 mice). Gray indicates the stimulation period. 130 vs. 20 Hz: paired  $t$ -test or Wilcoxon matched-pairs signed rank test, two-sided, 0–3 s,  $P < 0.01$ ; 3–5 s,  $P < 0.05$ . **e** Comparing the firing rates within 10 s before, during, and after HFS (left) or LFS (right). Open circles indicate neurons with spontaneous firing ( $n = 5$ ), while filled circles represent those with a holding current of 20–50 pA to maintain stable firing ( $n = 3$ ). 130 Hz: Pre vs. Stim ( $P = 0.0156$ ), 20 Hz: Pre vs. Stim ( $P = 0.7422$ ), Wilcoxon matched-pairs signed rank test, two-sided. **f** Plots of the instantaneous frequency CV in the time windows shown in (**b**) ( $n = 8$  neurons from 5 mice). 130 Hz Base vs. Intra-1 ( $P = 0.0005$ ), Base vs. Intra-2 ( $P = 0.0016$ ). 20 Hz Base vs. Intra-1 ( $P = 0.6933$ ),

Base vs. Intra-2 ( $P = 0.8860$ ), paired  $t$ -test, two-sided. Data are represented as mean  $\pm$  SEM. (**g**) Left, schematic of STN DBS with bilateral drug administration in DD mice. Right, a representative sagittal section ( $n = 4$  mice) showing the position of cannula and electrode. Note that CTB-488 signals are restricted to the STN. Scale bar, 1 mm. **h** Representative changes in locomotion velocity within 60 s in response to STN DBS at 130 Hz before and 20 min after bilateral vehicle or bicuculline (BCC, 500  $\mu\text{mol}$ , i.e., 1  $\mu\text{l}$  with a concentration of 500  $\mu\text{M}$ ) administration to the STN. **i, j** Group data comparing the effects of DBS at 130 or 20 Hz on locomotion velocity before and after vehicle and BCC administration ( $n = 5$  mice). For (**i**) 130 Hz Ctrl: Pre vs. Stim ( $P = 0.0052$ ); Vehicle: Pre vs. Stim ( $P = 0.0011$ ), paired  $t$ -test, two-sided. 20 Hz Ctrl: Pre vs. Stim ( $P = 0.1875$ ), Vehicle: Pre vs. Stim ( $P = 0.4375$ ), Wilcoxon matched-pairs signed rank test, two-sided. For (**j**) 130 Hz Ctrl: Pre vs. Stim ( $P = 0.0052$ ), BCC: Pre vs. Stim ( $P = 0.8127$ ), paired  $t$ -test, two-sided. 20 Hz Ctrl: Pre vs. Stim ( $P = 0.0685$ ), paired  $t$ -test, two-sided; BCC: Pre vs. Stim ( $P = 0.3125$ ), Wilcoxon matched-pairs signed rank test, two-sided. NS, not significant;  $*P < 0.05$ ,  $**P < 0.01$ ,  $***P < 0.001$ . Source data are provided as a Source Data file. See also Supplementary Figs. 2–4.



specificity of GPe-STN PV axons in mediating the therapeutic effect of DBS. We bilaterally injected viruses to GPe in PV-Cre mice to allow specific expression of eArch3.0, a proton-pumping archaerhodopsin, in GPe PV neurons (Supplementary Fig. 7a). Local optic inhibition of PV axons at STN dramatically diminished the effect of electric HFS at 130 Hz on locomotion velocity and immobility time (Supplementary Fig. 7b–e). The velocity ratio (Stim/Pre) showed a substantial decrease with optic inhibition. LFS produced no effect on motor function with or without optic inhibition (Supplementary Fig. 7f–h).

Taken together, these results indicate that the inhibitory synaptic inputs from GPe play a crucial role in STN DBS, and further demonstrate that the activation of PV axons originating from GPe is both necessary and sufficient for the effect of high-frequency DBS.

### HFS of PV axons inhibits and desynchronizes firing of STN neurons

To measure spiking responses of STN neurons to optogenetic stimulation of PV axons, we performed *in vivo* extracellular recordings from awake, free-moving mice. Recording electrodes with optic fibers were implanted into both sides of the STN (Fig. 4a) to obtain single-unit recording (Fig. 4b, c) during optic stimulation at 130 or 20 Hz in PV-Cre mice. Consistent with the results from acute slice recording with electric stimulation, optic HFS, but not LFS, reduced the firing rate of STN neurons (Fig. 4d, e). The baseline firing rate of recorded units fluctuated with an average CV less than 0.2, we therefore considered changes in firing rate more than 20% as effective responses. LFS at 20 Hz showed no significant change in the firing rates. However, in

**Fig. 3 | Activation of axons from GPe PV neurons is necessary and sufficient for DBS effect.** **a** Schematic of bilateral virus injections and bilateral implantation of optic fibers for optogenetic activation of GPe axons in DD mice. **b** Average velocity (bin size: 5 s) before (Pre), during (Stim, blue), and after (Post) 130 Hz HFS of GPe axons (oChIEF,  $n = 6$  mice; tdTomato,  $n = 6$  mice). **c**, Group data comparing the average velocity within 30 s before, during, and after the optogenetic HFS of GPe axons at STN. Note the increase in locomotion velocity in mice with oChIEF/tdTomato expression ( $n = 6$  mice) but not those with tdTomato expression alone (control,  $n = 6$  mice). oChIEF: Pre vs. Stim ( $P = 0.0313$ ), Wilcoxon matched-pairs signed rank test, two-sided; tdTomato: Pre vs. Stim ( $P = 0.6684$ ), paired  $t$ -test, two-sided. **d–f** Similar experiments as in **a–c** but with virus injection in PV-Cre mice to allow Cre-dependent expression of oChIEF/mCherry in GPe PV-positive neurons. Note the increase in velocity of mice with oChIEF expression ( $n = 12$  mice) but not those with mCherry alone ( $n = 8$  mice). For (**f**) oChIEF: Pre vs. Stim ( $P = 0.0005$ ), mCherry: Pre vs. Stim ( $P = 0.5469$ ), Wilcoxon matched-pairs signed rank test, two-sided. **g–i** Similar experiments as in (**d–f**) but with Cre-off virus injections that allow a selective expression of oChIEF in GPe non-PV neurons. Note that optogenetic activation of non-PV axons at either 130 or 20 Hz produced no change in

locomotion velocity ( $n = 7$  mice). For (**i**) oChIEF-130 Hz: Pre vs. Stim ( $P = 0.9543$ ), oChIEF-20 Hz: Pre vs. Stim ( $P = 0.2290$ ), paired  $t$  test, two-sided. **j** Representative images showing the expression of mCherry and PV immunosignals in PV-Cre mice with two types of viruses (Cre-on DIO and Cre-off DO). Scale bar, 100  $\mu\text{m}$ . **k** Left, percentage of PV-positive cells in mCherry-expressing cells with the Cre-on virus injection ( $n = 5$  mice). Right, percentage of PV-negative cells in mCherry-expressing cells with the Cre-off virus injection ( $n = 6$  mice). **l** Schematic of virus injections for bilateral ablation of PV neurons and STN DBS in DD mice. **m** A complete loss of PV-positive cells in GPe 3–5 weeks after the virus injection ( $n = 5$  mice). Scale bar, 500  $\mu\text{m}$ . **n** Group data comparing the average velocity within 10 min of PV-Cre DD mice ( $n = 11$  mice) and PV-ablated DD mice ( $n = 12$  mice). Unpaired  $t$ -test, two-sided,  $P = 0.5792$ . **o** Representative traces showing the effect of 130- or 20-Hz STN DBS on the locomotion velocity of mice with PV cell ablation. **p** Group data comparing the average velocity within 60 s before, during, and after the DBS ( $n = 12$  mice). 130 Hz: Pre vs. Stim ( $P = 0.2925$ ), paired  $t$ -test, two-sided; 20 Hz: Pre vs. Stim ( $P = 0.5186$ ), Wilcoxon matched-pairs signed rank test, two-sided. NS, not significant;  $*P < 0.05$ ,  $***P < 0.001$ . Data are represented as mean  $\pm$  SEM. Source data are provided as a Source Data file. See also Supplementary Figs. 5 and 6.

response to 130-Hz light stimulation, approximately one third (34.4%,  $n = 11/32$ ) of the units showed decreases in their firing rates (Fig. 4f, g). The spiking activity in majority of the recorded units was unaffected (59.38%,  $n = 19/32$  neurons), with only two units showing an increase in their firing rate (Fig. 4f).

To examine the synchrony of STN neuron activity, we analyzed the temporal distance of individual spike to the nearest spike in paired units (inter cross-unit interval, ICUI), as well as the CV of ICUI in paired units and ISI in individual units (11 units with light-induced inhibition at 130 Hz) (Fig. 4h). Distinct from 20 Hz, 130-Hz light stimulation increased both the temporal distance and the CV (Fig. 4i–l). Interestingly, as compared to pre-stimulation (130 Hz), the temporal distance and the CV during the 30-s period of post-stimulation were also significantly higher (Fig. 4j, l), suggesting a long-lasting effect of the optic HFS, possibly due to a role of prolonged AR from PV axons. We further analyzed the local field potential (LFP) and found that 130-Hz but not 20-Hz optic stimulation significantly reduced low beta oscillations in DD mice (Supplementary Fig. 8a–c), also supporting a role of HFS in reducing network synchronization at low frequencies. Similar optogenetic behavioral tests and LFP recording at STN were performed on rats with ipsilateral DD or control animals. Consistent with previous findings<sup>28</sup>, an enhancement of beta oscillation was observed in DD rats (Supplementary Fig. 8d–h). Optic activation of GPe-STN axons at 130 Hz (but not 20 Hz) diminished the power of high beta, dramatically increased the locomotion velocity, and decreased the immobility time (Supplementary Fig. 8i–o), similar to the results observed in mice.

We further examined the synaptic responses of STN neurons to optic stimulation of PV axons (Fig. 5a, b). Similar to the findings with electric stimulation in STN slices, the total charge of the IPSCs evoked by 130-Hz light stimulation was significantly greater than that at 20 Hz, but only within a few seconds after the stimulation onset ( $\sim 6$  s). Analysis of the SR and AR components revealed that the significant difference in SR charge occurred in a very short time window ( $\sim 2$  s) at the beginning of the light stimulation, while the AR ratio and the basal current displayed significant differences during the whole period of stimulation (Fig. 5c–f). Similar to Fig. 1g, overlay of the current traces induced by individual optic pulses during the HFS reveals a progressive reduction of evoked IPSCs but a progressive increase in AR events. For LFS at 20 Hz, however, individual optic pulses could reliably evoke SR-related IPSCs during the entire period of stimulation (Fig. 5g). Consistent with the behavioral results, the AR ratio under 45-Hz optic stimulation falls between those observed with HFS and LFS, suggesting a positive correlation between the strength of AR and the therapeutic effect of DBS (Supplementary Fig. 6g–m).

Next, we examined spiking responses of STN neurons to 10-s optic stimulation of GPe PV axons in slices perfused with low- $\text{Ca}^{2+}/\text{Mg}^{2+}$  ACSF. We observed a reduction in the AP frequency in responses to

HFS. Unlike the experiments in vivo, optic LFS also substantially inhibited STN neurons, most likely attributable to the high power of light source and the selection of regions with dense PV axons for recording. Similar to the observations with electric stimulation in slices (Fig. 2) and those in vivo (Fig. 4), the CV of instantaneous frequency increased during HFS but not LFS (Fig. 5h–m). Hence, HFS of PV axons alone produces both inhibition and desynchronization of the spiking activity of STN neurons.

### AR strength at GPe PV axons regulates the DBS effect

The occurrence of SR and AR is determined by different levels of presynaptic  $\text{Ca}^{2+}$  concentrations, and mediated by distinct  $\text{Ca}^{2+}$  sensors, including synaptotagmin-1 (Syt1) and Syt7, respectively<sup>29</sup>. Next, we sought to manipulate the AR strength at GABAergic synapses from GPe PV neurons onto STN neurons by chelating background  $\text{Ca}^{2+}$  or downregulating the  $\text{Ca}^{2+}$  sensor to examine the role of AR in DBS effect.

We first bilaterally applied the membrane-permeable  $\text{Ca}^{2+}$  chelator EGTA-AM through local infusion at STN that could selectively reduce AR at hippocampal cholecystikinin (CCK)-expressing interneurons synapses onto granule neurons in slice preparations<sup>30</sup>. In our experiments, we found that indeed bath application of 200  $\mu\text{M}$  EGTA-AM substantially reduced the total charge, AR charge, and basal currents triggered by 130-Hz light stimulation, but it also reduced the SR charge (Fig. 6a–d). We then performed similar experiments shown in Fig. 3d–f, but with bilaterally implanted guide cannulas that allow alternative optic stimulation and drug application at the STN of PV-Cre mice (Fig. 6e, see “Methods”). In PV-Cre DD mice, 20 min after the application of EGTA-AM (0.5  $\mu\text{mol}$ ), the therapeutic effect of 130-Hz optic stimulation on locomotion was dramatically reduced (Fig. 6f–h). Light stimulation at 20 Hz produced no obvious effect on locomotion either before or after EGTA-AM administration. In control experiments, local infusion of vehicle showed no discernible change in the effects of HFS or LFS (Fig. 6f–h).

Previous studies showed that knocking down Syt1 would dramatically enhance AR<sup>31</sup>. We then specifically downregulate the expression of this  $\text{Ca}^{2+}$  sensor in GPe PV neurons. Using a Cre-LoxP and Flp-FRT combinatory system, we injected viruses into GPe and allow selective expression of Syt1 shRNA and oChIEF in PV neurons (Fig. 7). In STN slices with Syt1 downregulation, we detected lower amplitude of SR events during light stimulation at both 130 Hz and 20 Hz in one third of the recorded STN cells (Fig. 7a, b). Group data from all recorded cells with Syt1 downregulation revealed similar differences in the total IPSC charge between HFS and LFS (Fig. 7c), but a significant increase in AR ratio during LFS (Fig. 7e, g), reaching a comparable AR strength to that during HFS across the whole period of stimulation. The increase in AR ratio reflects a decrease in SR strength (Fig. 7d), which is consistent with the role of Syt1 in mediating the SR<sup>29,31</sup>.

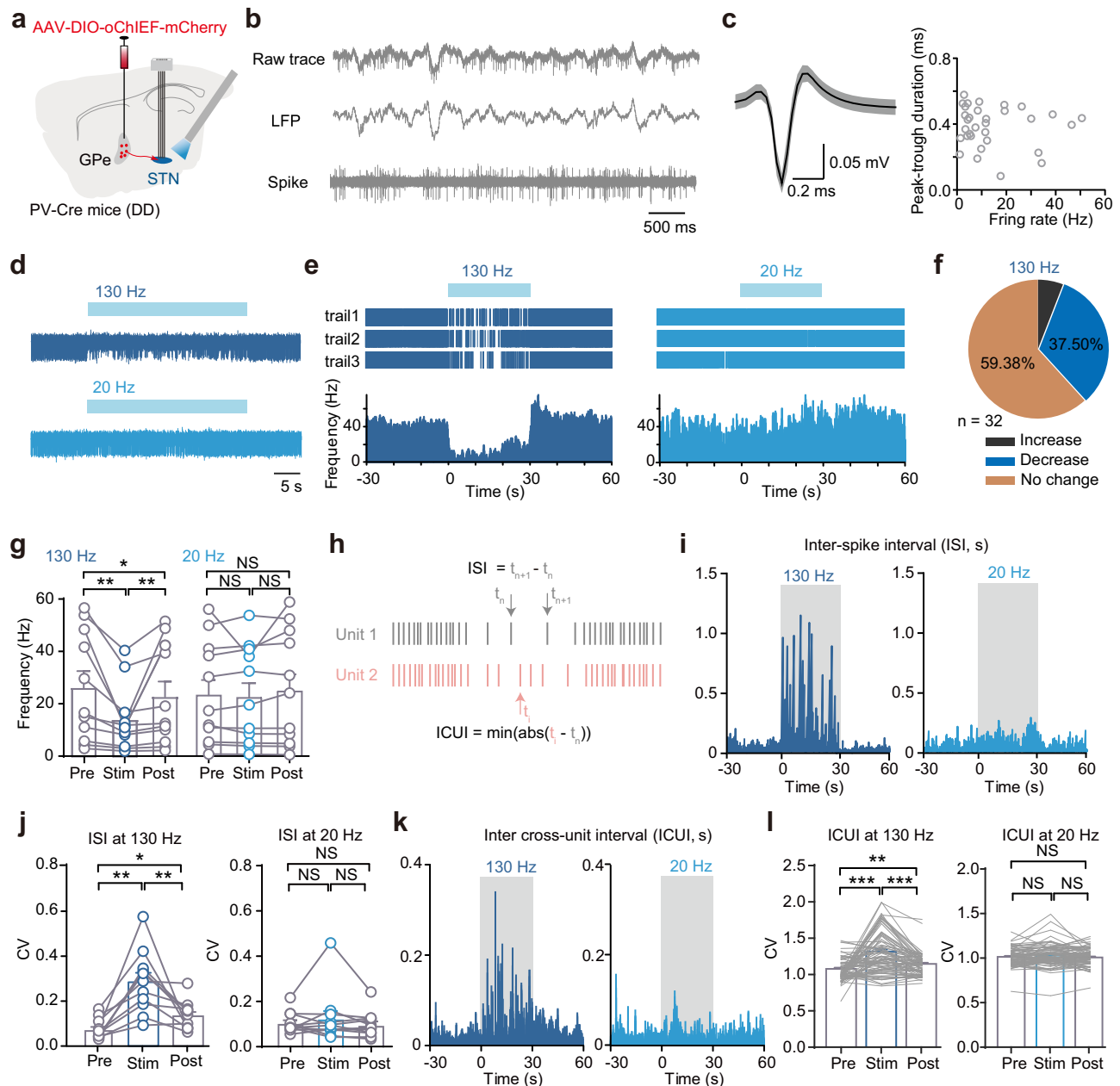
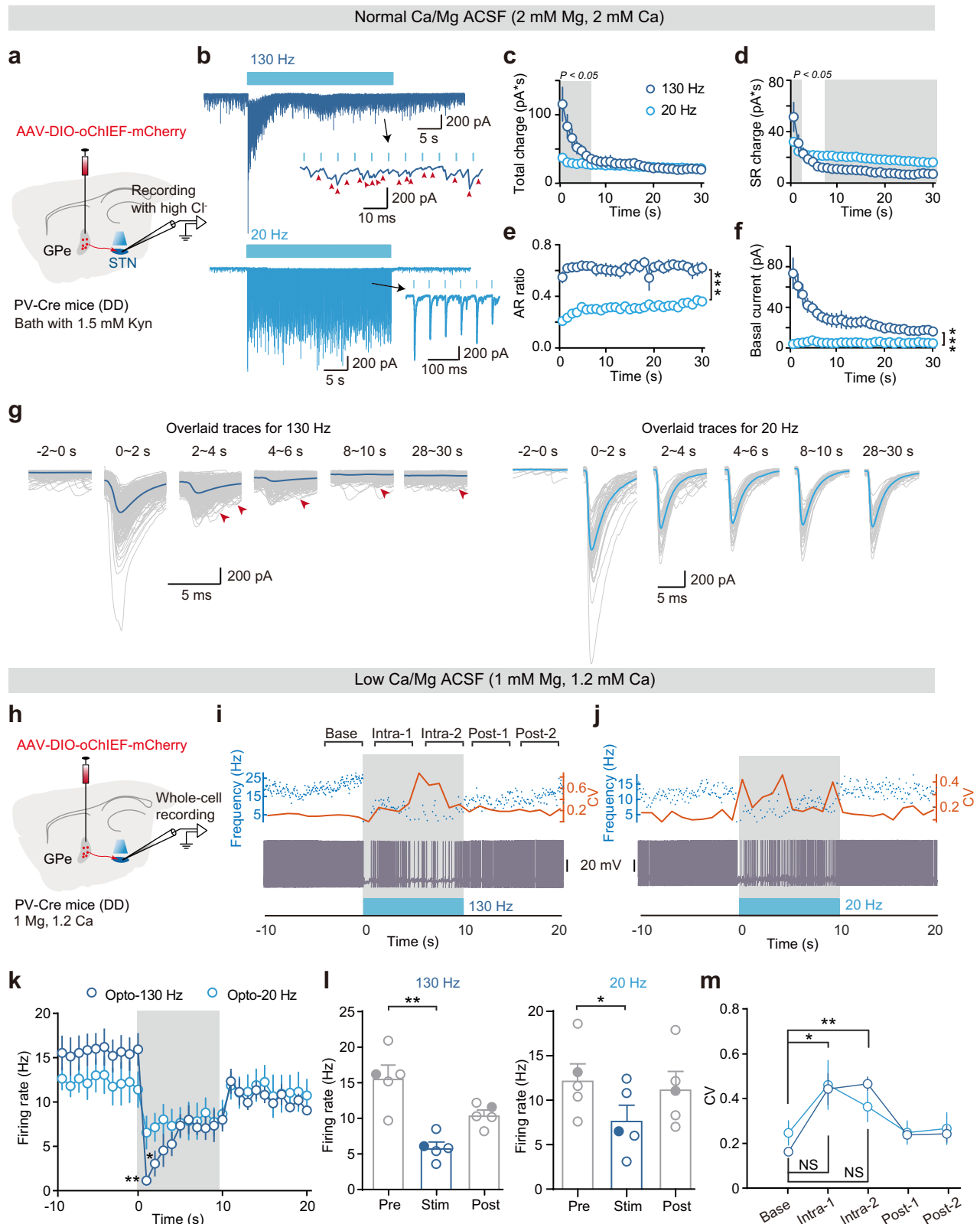


**Fig. 4 | HFS of PV axons inhibits and desynchronizes firing of STN neurons in vivo.** **a** Schematic of bilateral single-unit recording in STN with optogenetic stimulation of GPe PV axons in vivo. **b** Representative single-unit recording from STN cells showing the raw trace (top), LFP (middle), and spikes (bottom). **c** Left, a representative extracellular spike. Right, plots of the spike duration versus the firing rates of individual cells ( $n = 32$  single units). **d** Two example traces from a single unit showing differential effect of HFS and LFS. **e** Three different trials of light stimulation (top) and the average instantaneous frequency (bottom) in the same unit shown in **(d)**. **f** Pie chart showing the percentage of units with different responses to light stimulation of PV axons. **g** Group data showing that single units with light-induced inhibition at 130 Hz exhibit no significant change in their firing rates with 20 Hz light stimulation ( $n = 11$  units from 8 mice). 130 Hz: Pre vs. Stim ( $P = 0.0010$ ), Stim vs. Post ( $P = 0.0010$ ), Pre vs. Post ( $P = 0.0322$ ), Wilcoxon matched-pairs signed rank test, two-sided; 20 Hz: Pre vs. Stim ( $P = 0.5044$ ), Stim vs. Post ( $P = 0.2716$ ), and Pre vs. Post ( $P = 0.3168$ ), paired  $t$ -test, two-sided.

**h** Calculation of the inter-spike interval (ISI) of a single unit and the inter cross-unit interval (ICUI) between two nearest spikes from two single units. **i** Representative ISI of a single unit before, during and after optogenetic HFS (left) and LFS (right). **j** Group data of CV of the ISI ( $n = 11$  units from 8 mice). 130 Hz: Pre vs. Stim ( $P = 0.0010$ ), Wilcoxon matched-pairs signed rank test, two-sided; Stim vs. Post ( $P = 0.0087$ ), paired  $t$ -test, two-sided; Pre vs. Post ( $P = 0.0137$ ), Wilcoxon matched-pairs signed rank test, two-sided. 20 Hz: Pre vs. Stim ( $P = 0.8984$ ), Stim vs. Post ( $P = 0.2783$ ), and Pre vs. Post ( $P = 0.5195$ ), Wilcoxon matched-pairs signed rank test, two-sided. **k** Representative ICUI between two units before, during, and after optogenetic HFS (left) and LFS (right). **l** Group data of CV of the ICUI ( $n = 82$  paired units from 8 mice). 130 Hz: Pre vs. Stim ( $P < 0.0001$ ), Stim vs. Post ( $P < 0.0001$ ), and Pre vs. Post ( $P = 0.0079$ ); 20 Hz: Pre vs. Stim ( $P = 0.2455$ ), Stim vs. Post ( $P = 0.2789$ ), and Pre vs. Post ( $P = 0.7862$ ), Wilcoxon matched-pairs signed rank test, two-sided. \* $P < 0.05$ , \*\* $P < 0.01$ , \*\*\* $P < 0.001$ . Data are represented as mean  $\pm$  SEM. Source data are provided as a Source Data file. See also Supplementary Fig. 8.

As expected, 130-Hz optic stimulation of PV axons with Syt1 downregulation increased the locomotion velocity and decreased the percentage of immobility time (Pre  $75.59 \pm 4.44\%$  vs. Stim  $49.20 \pm 7.59\%$ , paired  $t$ -test, two-sided,  $P = 0.0004$ ) of the PV-Cre DD

mice. Remarkably, 20-Hz optogenetic stimulation also significantly increased the locomotion velocity and decreased the percentage of immobility time (Pre  $73.71 \pm 6.14\%$  vs. Stim  $53.24 \pm 6.32\%$ , paired  $t$ -test, two-sided,  $P < 0.0001$ ), distinct from the failure of LFS in non-specific



control (NC) shRNA group (Fig. 7h–m and Supplementary Movie 3). These experiments show that an increase in the AR strength produces a beneficial effect with LFS of GPe PV axons on locomotion of DD mice.

In summary, our findings suggest a crucial role of asynchronous GABA release from GPe PV neurons in mediating the therapeutic effect of high-frequency DBS at STN. An enhancement of GABAergic input, particularly the AR strength, may substantially improve the efficacy of

DBS even at low frequencies. Our results also suggest that the AR strength could be considered as a potential biomarker for optimizing DBS parameters.

## Discussion

We identified that the activation of PV axons, but not non-PV axons, from the GPe by high-frequency DBS is both necessary and sufficient for

**Fig. 5 | HFS of PV axons triggers AR, inhibits, and desynchronizes firing of STN neurons in vitro.** **a** Schematic showing optogenetic stimulation of PV axons from GPe and IPSC recording with high-Cl<sup>-</sup> pipette solution in STN slices of DD mice. **b** Representative current traces of IPSCs evoked by long-lasting trains of optogenetic HFS (130 Hz) or LFS (20 Hz), similar to experiments with electric stimulation shown in Fig. 1. Red arrowheads indicate AR events. Note that robust AR events occurred during optic HFS. **c–f** Group data showing changes in the total charge, SR charge, AR ratio, and basal current of the evoked IPSCs during the optic HFS and LFS ( $n = 15$  neurons from 8 mice). Gray, time points with significant differences. For **(c)** 130 vs. 20 Hz, 0–7 s,  $P < 0.05$ ; for **(d)** 0–2 and 8–30 s,  $P < 0.05$ , Wilcoxon matched-pairs signed rank test, two-sided. For **(e, f)** 130 vs. 20 Hz,  $P < 0.0001$ , two-way ANOVA without adjustments. **g** Gray, overlaid current traces before the stimulation onset (–2 to 0 s) and those evoked by individual optic pulses during indicated time periods of stimulation (2 s each). Blue, the average traces. Red arrowheads indicate AR events. **h**, Examination of the effect of optic stimulation on firing rates of STN neurons (with normal pipette solution) with a more physiological level of Ca<sup>2+</sup> (1.2 mM) and Mg<sup>2+</sup> (1 mM) in the bath. Example current-clamp

recording showing the effects of optogenetic HFS (**i**) and LFS (**j**) on spontaneous firing of STN neurons. Top, plots of the instantaneous frequency of APs and its CV (bin size: 1 s). Time windows (4 s) before, during, and after the stimulation were shown for data analysis in **(m)**. **k** Group data showing changes in the firing rates in response to optogenetic HFS and LFS over time ( $n = 5$  neurons from 3 mice). Gray indicates the stimulation period. 130 vs. 20 Hz, Wilcoxon matched-pairs signed rank test or paired  $t$ -test, two-sided, 1–3 s,  $P < 0.05$ . **l** Comparing the firing rates within 10 s before, during, and after optogenetic HFS (left) or LFS (right). Open circles indicate neurons with spontaneous firing ( $n = 4$ ), while filled circles represent those with a holding current of 50 pA to maintain stable firing. 130 Hz: Pre vs. Stim ( $P = 0.0058$ ); 20 Hz: Pre vs. Stim ( $P = 0.0301$ ), paired  $t$ -test, two-sided. **m** Plots of the instantaneous frequency CV in the time windows shown in **(i)** ( $n = 5$  neurons from 3 mice). 130 Hz: Base vs. Intra-1 ( $P = 0.0101$ ), Base vs. Intra-2 ( $P = 0.0024$ ); 20 Hz: Base vs. Intra-1 ( $P = 0.1377$ ), Base vs. Intra-2 ( $P = 0.0527$ ), paired  $t$ -test, two-sided. NS, not significant; \* $P < 0.05$ , \*\* $P < 0.01$ , \*\*\* $P < 0.001$ . Data are mean  $\pm$  SEM. Source data are provided as a Source Data file. See also Supplementary Fig. 6.

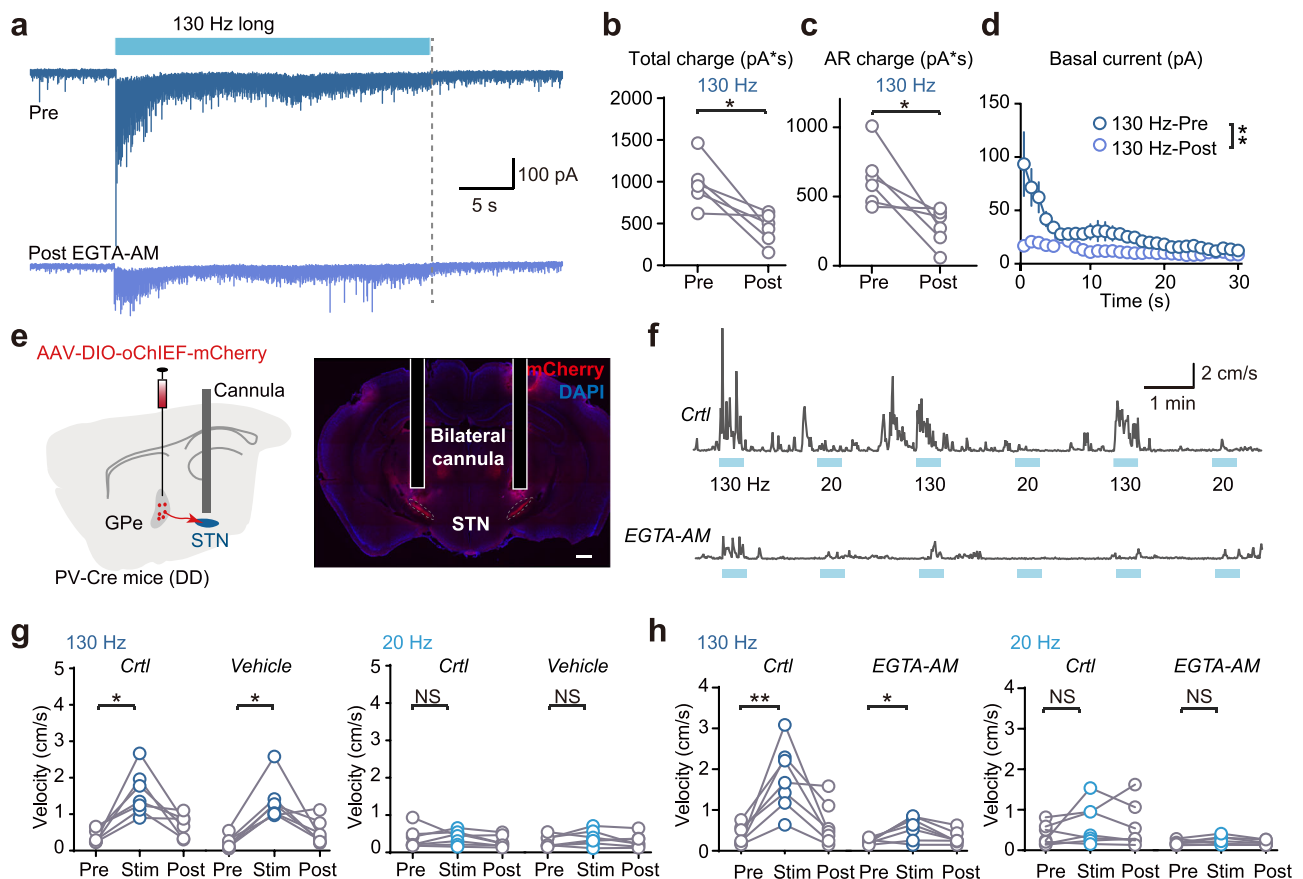


**Fig. 6 | Reducing AR strength diminishes the beneficial effect of PV axon HFS.** **a** Representative traces of IPSCs evoked by long-lasting trains of optic HFS before (top) and 20 min after 200  $\mu$ M EGTA-AM (bottom) application in the bath. Group data of the total charge (**b**), AR charge (**c**), basal current (**d**) of evoked IPSCs before and after the application of 200  $\mu$ M EGTA-AM ( $n = 6$  neurons from 4 mice). For **(b)** ( $P = 0.0149$ ) and **(c)** ( $P = 0.0258$ ), paired  $t$ -test, two-sided. For **(d)** ( $P = 0.0053$ ), two-way ANOVA without adjustments. **e** Left, schematic of bilateral virus injections and bilateral cannula implantation for drug administration. Right, a representative image ( $n = 4$  mice) showing the position of the two cannulas above the STN. Scale bar, 500  $\mu$ m. **f** Representative changes in locomotion velocity in response to optic stimulation of PV axons from GPe at 130 or 20 Hz before and 20 min after bilateral

EGTA-AM (500  $\mu$ M; i.e., 0.5  $\mu$ l with a concentration of 1 mM) administration to the STN. **g, h** Group data comparing the effects of optic stimulation on locomotion velocity before and after vehicle ( $n = 7$  mice) and EGTA-AM administration ( $n = 7$  mice). For **(g)** 130 Hz Ctrl: Pre vs. Stim ( $P = 0.0156$ ), Vehicle: Pre vs. Stim ( $P = 0.0156$ ), Wilcoxon matched-pairs signed rank test, two-sided. 20 Hz Ctrl: Pre vs. Stim ( $P = 0.4688$ ), Wilcoxon matched-pairs signed rank test, two-sided; Vehicle: Pre vs. Stim ( $P = 0.1831$ ), paired  $t$ -test, two-sided. For **h**, 130 Hz Ctrl: Pre vs. Stim ( $P = 0.0040$ ), EGTA-AM: Pre vs. Stim ( $P = 0.0178$ ); 20 Hz Ctrl: Pre vs. Stim ( $P = 0.2051$ ), EGTA-AM: Pre vs. Stim ( $P = 0.2485$ ), paired  $t$ -test, two-sided. Data are represented as mean  $\pm$  SEM. NS, not significant; \* $P < 0.05$ , \*\* $P < 0.01$ . Source data are provided as a Source Data file.

the beneficial effect of DBS at STN. We found that HFS desynchronizes GABA release from GPe PV axons and consequently the spiking activity of STN neurons, a potential mechanism for the therapeutic effect of high-frequency DBS. These results further suggest that the AR strength

at synapses from GPe PV neurons to STN cells could be a promising biomarker or reference for optimizing the DBS parameters.

In our experiments, we detected robust AR of both GABA and glutamate in response to prolonged 130-Hz HFS (up to 30 s in

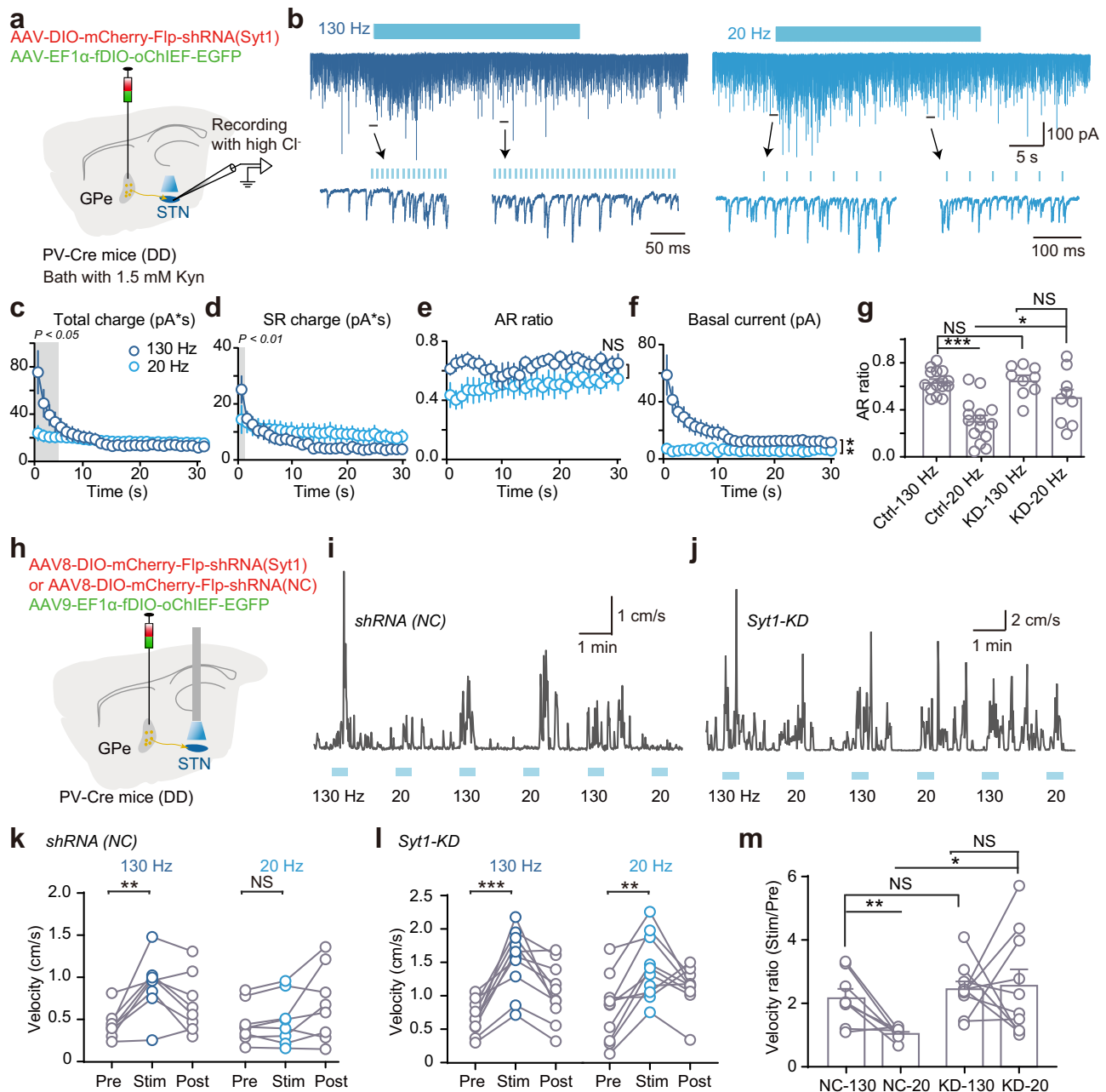


**Fig. 7 | LFS of PV axons also produces beneficial effect when AR strength is enhanced.** **a** Schematic of bilateral virus injections for selective expression of shRNA (Syt1) and oChIEF in GPe PV neurons and IPSC recording from STN slices of DD mice. **b** Representative current traces of IPSCs evoked by long-lasting trains of optic HFS or LFS with Syt1 down-regulation. Insets, expanded traces for clarity. **c–f** Group data showing changes in the total charge, SR charge, AR ratio, and basal current of the evoked IPSCs during optic HFS or LFS with Syt1 KD ( $n = 9$  neurons from 4 mice). Gray, time points with significant differences. Paired  $t$ -test or Wilcoxon matched-pairs signed rank test for (**c**, **d**) (two-sided): 130 vs. 20 Hz in (**c**) 0–4 s,  $P < 0.05$ ; in (**d**) 0–1 s,  $P = 0.0039$ . For (**e**) ( $P = 0.1415$ ) and (**f**) ( $P = 0.0094$ ), 130 vs. 20 Hz, two-way ANOVA without adjustments. **g** Group data comparing the AR ratio of IPSCs in control (data from Fig. 5e,  $n = 15$  neurons from 8 mice) and Syt1 KD mice ( $n = 9$  neurons from 4 mice). Ctrl: 130 vs. 20 Hz ( $P < 0.0001$ ); KD: 130 vs. 20 Hz ( $P = 0.2267$ ), paired  $t$ -test, two-sided. Ctrl-130 vs. KD-130 ( $P = 0.7797$ ), Ctrl-20 vs. KD-20 ( $P = 0.0306$ ), unpaired  $t$ -test, two-sided. **h** Schematic of virus injections for selective expression of Syt1 shRNA, or its non-specific control (NC) shRNA, with

oChIEF in GPe PV neurons and bilateral optic fiber implantation in STN of DD mice. Representative behavior test showing increases in locomotion velocity in response to optic stimulation in mice with selective expression of the NC shRNA (**i**) or with Syt1 KD (**j**) in GPe PV cells. **k** Group data comparing the average velocity within 30 s before, during, and after the optic stimulation with the NC shRNA ( $n = 8$  mice). Only HFS produced an increase in velocity, but not LFS. 130 Hz: Pre vs. Stim ( $P = 0.0039$ ); 20 Hz: Pre vs. Stim ( $P = 0.2747$ ), paired  $t$ -test, two-sided. **l** Similar to (**k**) but with Syt1 KD. Note the locomotion velocity increases during both HFS and LFS ( $n = 10$  mice). 130 Hz: Pre vs. Stim ( $P = 0.0001$ ); 20 Hz: Pre vs. Stim ( $P = 0.0010$ ), paired  $t$ -test, two-sided. **m** Group data comparing the ratio of locomotion velocity during stimulation (Stim) to that before stimulation (Pre) (NC,  $n = 8$  mice; KD,  $n = 10$  mice). NC-130 vs. NC-20 ( $P = 0.0092$ ), KD-130 vs. KD-20 ( $P = 0.8695$ ), paired  $t$ -test, two-sided. NC-130 vs. KD-130 ( $P = 0.4627$ ), NC-20 vs. KD-20 ( $P = 0.0185$ ), unpaired  $t$ -test, two-sided. Data are represented as mean  $\pm$  SEM. NS, not significant; \* $P < 0.05$ , \*\* $P < 0.01$ , \*\*\* $P < 0.001$ . Source data are provided as a Source Data file.

duration). Previous studies revealed that the AR strength at both excitatory and inhibitory synapses depends on the stimulation intensity, the higher frequency or more stimulation pulses (i.e., longer time), the stronger AR would occur<sup>16,17,19</sup>. Thus, AR events may not be obvious during brief train of HFS, 1 s, for example<sup>32</sup>. A previous study also revealed that long-lasting HFS also increases the frequency CV of STN neurons, while brief HFS only induces inhibition<sup>33</sup>. Our results indicate that the initial brief inhibition and the later desynchronized activity could be attributed to the occurrence of early strong SR and later AR, respectively. Therefore, findings in this study highlight the necessity of delivering prolonged stimulation, similar to the long-lasting DBS for human patients, to explore the underlying mechanisms of DBS.

Whether high-frequency DBS excites or inhibits STN neurons remains an open question. There is no doubt that DBS will excite STN neurons near the electrode. Much larger population of STN neurons is not directly excited, they rather receive synaptic inputs from directly stimulated axons and their arborizations (due to action potential propagation). In this case, the sign of modulation, excitation, or inhibition depends on the net effect of integrated excitatory and inhibitory postsynaptic potentials (EPSPs and IPSPs). Previous studies showed that activation of excitatory synaptic inputs, including those from motor cortex (M1) and parafascicular (PF) nucleus<sup>34,35</sup> or inhibitory synaptic inputs (mainly from GPe)<sup>24,25</sup> relieves dyskinesia in DD mice. It has been proposed that DBS-induced AP backpropagation along axons of the cortico-STN hyperdirect pathway would desynchronize cortical pyramidal cells and contribute to the beneficial effect of DBS<sup>36–39</sup>. In our experiments, however, blocking GABA<sub>A</sub> receptors in STN or genetic ablation of GPe PV cells completely abolished the DBS effects, confirming an essential contribution of inhibitory inputs. Under these experimental conditions, DBS at STN still activates glutamatergic inputs, but the motor deficits showed no obvious alleviation, suggesting that the activation of excitatory synaptic inputs alone cannot achieve the beneficial effects. Our results agree well with a previous study in mice showing that surgical removal of the primary motor cortex failed to eliminate the therapeutic effect of STN DBS<sup>40</sup>. We speculate that while the recruited cortical projection neurons are desynchronized through unreliable backpropagation of axonal APs<sup>36,37,39</sup> and/or recruiting somatostatin-expressing neurons<sup>41</sup>, DBS also activates GPe axon terminals at STN and desynchronizes spiking activity of STN neurons to exert their effects on motor functions. It is also highly possible that desynchronized cortical projection neurons during DBS exerts their therapeutic effect through GPe-mediated indirect pathway. A theoretical model of STN neurons based on single-neuron activity recordings from PD patients during DBS also shows that inhibitory synaptic inputs suppress neuronal activity and thereby regulate neural network activity<sup>42</sup>. Abnormal hyperexcitability and burst firing observed at STN in PD patients<sup>43,44</sup> also requires GABAergic synaptic inputs to tick the balance back to a physiological level. A recent study<sup>45</sup> also reveals that HFS at STN induces sonic hedgehog (Shh) release, which regulates neuronal spiking activity and contribute to the relief of Parkinsonian motor deficits. It remains to be further examined whether the effect of Shh could also be mediated by GABA AR.

Local administration of GABA<sub>A</sub> receptor agonist muscimol or lidocaine has been shown to alleviate the dyskinesia in both PD patients<sup>46</sup> and non-human primate model<sup>47</sup>, indicating the importance of inhibition during DBS at STN. In DD mouse model, an early study showed that optogenetic inhibition of STN neurons produced no alleviation of locomotion deficits<sup>34</sup>. In contrast, studies in rat Parkinsonian model demonstrated that optogenetic inhibition of STN neurons improves motor function only in forelimb movements<sup>48</sup> and alleviates levodopa-induced dyskinesia<sup>49</sup>. The inconsistency of these findings may result from differences in opsin efficiency and inhibition efficacy, casting doubt on the role of STN inhibition.

With an ultrafast opsin, the Chronos, optogenetic stimulation of STN neurons could relieve the dyskinesias of DD mice, presumably through feedback inhibition of a subpopulation of STN cells without opsin expression<sup>50</sup>. The major source of inhibition comes from GPe neurons, whose functions in motor control have been extensively studied<sup>51–53</sup>. PV-expressing neurons, the predominant cell type in GPe, are closely associated with motor functions such as walking<sup>24,25,51</sup>. Genetic ablation of GPe PV neurons in our experiments not only suppresses the spontaneous locomotion (Supplementary Fig. 5n–p) but also diminishes the effect of DBS. Recent studies also found that activation of PV neurons and simultaneous inhibition of Lhx6-positive neurons are required to achieve long-lasting improvement of motor functions<sup>24,54</sup>. In the case of DBS at STN, axons from both GPe PV- and Lhx6-positive neurons should be activated simultaneously, but our results reveal a critical role of PV axons but not non-PV axons in the DBS beneficial effect. Our experiments with optogenetic activation and cell ablation indicate that the activation of GPe-STN PV axons is both necessary and sufficient for the DBS therapeutic effects (Fig. 3). Previous studies suggest that oChIEF-mediated photocurrents may accumulate during optic HFS, despite their relatively short decay time constant<sup>55–57</sup>. The AR ratio of IPSCs evoked by optic HFS at 130 Hz (Fig. 5e) is slightly higher than that of electric HFS (Fig. 1j), suggesting a contribution of accumulated photocurrents to the increased AR ratio. In neocortical axons, a single depolarizing pulse can only trigger one axonal AP<sup>58</sup>, subthreshold depolarization can shape the AP waveform but cannot trigger synaptic release<sup>59</sup>, possibly due to the expression of high-threshold Ca<sup>2+</sup> channels at the axon terminals. Therefore, it remains to be further examined whether photocurrent-induced subthreshold depolarization affects axonal AP frequency and synaptic transmission in GPe PV axons.

In agreement with previous findings indicating an important role of HFS-induced AR in regulating the temporal precision of AP generation<sup>16,18,19</sup>, our results show that both electric and optic HFS evoke AR of neurotransmitters and increase the CV of spikes, reflecting desynchronization of spiking activity in postsynaptic STN neurons. Indeed, DBS at STN in PD patients suppresses beta band network activity<sup>20,60</sup> and disrupt pathological burst firing of STN neurons<sup>44,61</sup>. Direct measurements of changes in the synchrony of STN neurons during the DBS treatment using high-throughput single-unit recording can be carried out in future studies to further examine the role of presynaptic GABA AR and postsynaptic spiking synchronization in the therapeutic effect of DBS. Except the initial period of HFS during which both SR and AR contribute to the inhibition, the AR ratio or basal current during HFS remain greater than those during LFS, matching well with the persistent therapeutic effects during prolonged high-frequency DBS. Moreover, an increase in AR strength induced by knocking down Syt1 from GPe PV neurons enable LFS to produce a beneficial effect, suggesting that low-frequency DBS could also exert a therapeutic effect as long as the AR strength reaches a threshold. Therefore, the AR strength could be considered as a potential biomarker for optimizing DBS parameters in future studies. Given that recording neurotransmitter AR in human patients is not feasible, intracellular recording in acute brain slices from Parkinsonian model animals can be employed to measure AR strength and optimize DBS parameters for clinical application in PD patients. Furthermore, AR-based selection of DBS parameters may offer a promising strategy to refine variable frequency stimulation (VFS) and reduce the adverse effects associated with long-term high-frequency DBS.

## Methods

### Animals and dopamine-depletion model

Experimental animals were bred and used in accordance with the guidelines of the Institutional Animal Care and Use Committee of the Department of Laboratory Animal Science at Fudan University. The experimental protocols were approved by this committee

(2021)SITBR-001, FE21173). Animals were housed in standard conditions (with ambient temperature of 20–22 °C and humidity of 45–55%) with a libitum access to food and water, under a 12-h light-dark cycle. Wild-type mice (WT, C57 BL6/J) and Sprague-Dawley (SD) rats were obtained from Beijing Vital River Laboratory Animal Technology Co., Ltd. Additionally, PV-Cre mice (Stock No. 008069 IMSR JAX: 008069, Jackson Labs) were used for selective manipulation of GPe PV neurons and electrophysiological recordings. All mice (>8 weeks old) and SD rats (>6 weeks old) used in this study were males. Behavioral tests and electrophysiological recordings were conducted in mice between ages of 8 and 14 weeks and rats of 10–12 weeks. To examine the region of virus infection and verification of stimulating, recording, or drug application sites, we anesthetized the animals with intraperitoneal injection of 1% sodium pentobarbital (100 mg/kg of body weight) or Zoletil (50 mg/kg of body weight), followed by intracardial perfusion of saline and then 4% paraformaldehyde (PFA). Unless specifically stated, other animals were finally euthanized with CO<sub>2</sub>, followed by cervical dislocation.

To prepare the dopamine depletion (DD) mouse model of Parkinson's disease, we bilaterally injected 650–700 nl of 6-hydroxydopamine (6-OHDA) (5 µg/µl in 0.9% NaCl with 0.1% L-ascorbic acid, Sigma) into the medial forebrain bundle (MFB, coordinates from the bregma: AP –0.9 mm, ML ± 1.2 mm, DV –4.9 mm) at a rate of 100 nl/min in mice weighing over 20 g. Desipramine (25 mg/kg, Sigma) was intraperitoneally injected ~40 min before 6-OHDA administration to protect other monoaminergic neurons. Animals were carefully nursed after the 6-OHDA injection. Electrophysiological recordings or behavior tests were performed 4–6 days after dopamine depletion. Mice without 6-OHDA treatment were used as controls. To establish the DD rat model, we unilaterally injected 1.5 µl of 6-OHDA per site into the MFB (coordinates relative to the bregma: AP –3.8 mm, ML –1.6 mm, DV –8.2 and –8.6 mm) at a rate of 100 nl/min in 6-week-old rats. Two weeks after 6-OHDA injection, we administered apomorphine (0.5 mg/kg, Sigma, PHR2621) intraperitoneally to examine whether the model is successful. The success of the rat model is defined if the number of rotations is more than 10 turns per minute. Unilateral optic fibers and multichannel recording electrodes were implanted to the ipsilateral STN 4 weeks after virus injection. Rats with vehicle (0.1% L-ascorbic acid in saline) injection to the MFB were used as control. After all the experiments, we also performed immunostaining of striatum sections using TH antibody to further examine the success or failure of the DD model.

### Slice preparation

In each experimental group, mice of the same gender and similar age were randomly selected. Slices of the STN were obtained from control and DD mice. We cut parasagittal slices with an angle of 20° to preserve basal ganglia fibers<sup>62</sup>. Animals were anesthetized with 1% sodium pentobarbital (100 mg/kg of body weight) or Zoletil (50 mg/kg of body weight), followed by intracardial perfusion and decapitation. The brains were rapidly dissected out and immersed in an ice-cold, aerated (95% O<sub>2</sub> and 5% CO<sub>2</sub>) sucrose-based slicing solution, which is the normal artificial cerebrospinal fluid (ACSF) but with NaCl replaced by equimolar sucrose. Slices with a thickness of 300 µm were cut in the same solution using a vibratome (VT-1200S, Leica) and immediately transferred to a chamber filled with aerated ACSF. The slices were incubated at 35.5 °C for 40–60 min and then at room temperature until electrophysiological recording. For slice recording, we transferred individual slices to a recording chamber perfused with normal ACSF or ACSF containing specific blockers of neurotransmitter receptors at 34.0–34.5 °C. Recordings were performed under an infrared differential interference contrast (IR-DIC) microscope (BX-51WI, Olympus). We visualized cells and axon fibers using real-time DIC and epifluorescence imaging.

The normal ACSF contained (in mM) 126 NaCl, 2.5 KCl, 2 MgSO<sub>4</sub>, 2 CaCl<sub>2</sub>, 26 NaHCO<sub>3</sub>, 1.25 NaH<sub>2</sub>PO<sub>4</sub>, and 25 dextrose (315 mOsm, pH 7.4), and was bubbled with 95% O<sub>2</sub> and 5% CO<sub>2</sub> continuously.

### Electrophysiological Recordings

Unless otherwise stated, we performed whole-cell recordings from STN neurons. Glass pipettes had an impedance of 5–7 MΩ when filled with either normal internal solution (in mM, 140 K-Gluconate, 3 KCl, 2 MgCl<sub>2</sub>, 0.2 EGTA, 10 HEPES, 2 Na<sub>2</sub>ATP) or high-Cl<sup>–</sup> internal solution (72 K-Gluconate, 71 KCl, 2 MgCl<sub>2</sub>, 0.2 EGTA, 10 HEPES, 2 Na<sub>2</sub>ATP) with osmolarity of 285–295 mOsm and pH 7.20–7.25. Voltage or current clamp recordings were conducted using a MultiClamp 700B amplifier (Molecular Devices). Data acquisition was achieved using Power1401-3 (Cambridge Electronic Design, CED) and Spike2 software (Version 10, CED), with voltage and current signals filtered at 10 kHz and 3 kHz, respectively, and sampled at 50 kHz.

To examine the spontaneous firing and spiking responses to intracellular current injections, we recorded STN neurons using the normal internal solution. We obtained cell-attached recording initially and then ruptured the cell membrane to form whole-cell recording. Cells with spontaneous firing for at least 10 s at similar frequencies were included for data analysis (Supplementary Fig. 2h–j). To isolate the IPSCs, we added 1.5 mM kynurenic acid, an ionotropic glutamate receptor blocker, to the ACSF and used a high-Cl<sup>–</sup> internal solution. For EPSC recording in voltage clamp mode, we used the normal internal solution and held the recorded cell at –70 mV. In experiments with electric stimulation in STN slices, an isolator (ISO-Flex, AMPI) and bipolar electrodes were used to deliver stimulus trains (25–30 µA, 0.1 ms, 130 Hz or 20 Hz). The stimulation electrode was placed locally 100–150 µm away from the recorded cell. Long-lasting train stimulation (10 s or longer in train duration) was delivered to the tissue to evoke synaptic responses and examine spiking responses of STN neurons. For IPSC and EPSC recording with long-lasting train stimulation, 60-s interval was used to allow recovery of synaptic responses. To examine the effect of train stimulation at high and low frequencies with the same charge sizes of electric stimulation, we applied 1200 electric pulses in total and compared the evoked synaptic responses. To investigate the effect of HFS and LFS on spiking activity of STN neurons, we performed whole-cell current clamp recording (with pipettes filled with normal internal solution unless otherwise stated) to monitor spontaneous firing of STN neurons without any intracellular current injections but with trains of extracellular electric stimulation. In occasional cases, we injected constant currents (20–50 pA) to depolarize the membrane potential and allow persistent firing in the recorded neurons. Data from these manipulated cells were marked in figures and their corresponding legends. Experiments examining the effect of electric stimulation on spontaneous firing of STN neurons were also carried out in cell-attached mode (using pipettes filled with ACSF).

In experiments with long-term optogenetic stimulation (10 s for examination of STN spiking activity and 30 s for IPSC recording), a LED light source (473 nm, FL0117, FluoCa) was used to activate specific axons at either 130 Hz, 45 Hz, or 20 Hz. The duration of each light pulse was 1 ms, and the maximum intensity of continuous light output measured under the 40x objective was 45 mW. To examine whether GPe neurons expressing oChIEF could faithfully follow the stimulation frequencies of light pulses, we recorded oChIEF/mCherry-positive cells in the GPe and found that they were able to follow long-lasting light pulses at a frequency up to 130 Hz (n = 13 neurons, 135.8 ± 3.384 Hz). In response to 20 Hz light stimulation, GPe cells actually generated 1 to 3 APs per light pulse, resulting in a mean frequency at 36.04 ± 3.979 Hz (n = 13 neurons, Supplementary Fig. 5b–e). To detect light-evoked IPSCs in STN neurons, we performed whole-cell recording in brain slices with high-Cl<sup>–</sup> pipette solution, similar to the experiments with

electric stimulation. Slice preparation for optogenetic stimulation was carried out at least 18 h after *in vivo* optogenetic experiments.

In some experiments, PTX or BCC (50  $\mu$ M, Tocris) were added to the bath solution to block GABA<sub>A</sub> receptors, and incubation of slices with membrane permeable EGTA-AM (200  $\mu$ M, Thermo) would allow accumulation of EGTA in cells and thus reduce intracellular concentration of Ca<sup>2+</sup>. In experiments examining electrophysiological properties with a more physiological level of Ca<sup>2+</sup> and Mg<sup>2+</sup>, we reduced their concentration in the bath to 1.2 mM and 1.0 mM, respectively, while all other experimental conditions remained unchanged.

### Stereotaxic virus injections

All stereotaxic surgeries were conducted under isoflurane anesthesia, with a pre-anesthesia dosage of 3–4% followed by maintenance at 1–1.5% until completion of the surgery. To maintain the body temperature, we used a heating pad placed under the mouse body throughout the surgery procedure. After skull leveling, viruses were injected into the target brain region at a rate of 100 nl/min, with a volume of 250–300 nl per side for mice and 300 nl per site for rats. The injection needle was left in place for over 10 min to ensure complete diffusion. All viruses used in the study were allowed to express for at least 3–4 weeks.

We injected AAV<sub>2/8</sub>-hsyn-oChIEF-tdTomato (titer of  $4.8 \times 10^{12}$  vector genomes (vg) ml<sup>-1</sup>) bilaterally into GPe to express oChIEF non-specifically in GPe neurons, and activate oChIEF-expressing axons at STN using optic fibers implanted during the virus injection surgery. We used AAV<sub>2/8</sub>-hsyn-tdTomato as a control virus ( $1.41 \times 10^{13}$  vg ml<sup>-1</sup>), which expresses tdTomato alone, but not oChIEF. For optogenetic activation of PV or non-PV axons from GPe specifically, we injected Cre-dependent (Cre-on) virus AAV<sub>2/8</sub>-DIO-oChIEF-mCherry ( $1.65 \times 10^{13}$  vg ml<sup>-1</sup>) or Cre-off virus AAV<sub>2/8</sub>-DO-oChIEF-mCherry ( $1.33 \times 10^{13}$  vg ml<sup>-1</sup>) into GPe bilaterally in PV-Cre mice to allow expression of oChIEF in PV-positive neurons or non-PV neurons. AAV<sub>2/8</sub>-DIO-mCherry ( $1.76 \times 10^{13}$  vg ml<sup>-1</sup>) was used as a control virus. For specific optogenetic inhibition of GPe-STN PV axons, we bilaterally injected Cre-dependent viruses (AAV<sub>2/8</sub>-DIO-eArch3.0-eYFP,  $5.31 \times 10^{12}$  vg ml<sup>-1</sup>) into the GPe of PV-Cre mice.

In experiments manipulating the expression level of Syt1, we selectively knocked down Syt1 in PV neurons of GPe by injecting a mixture of two viruses, AAV<sub>2/8</sub>-DIO-mCherry-Flp-shRNA (Syt1) (titer of  $2.08 \times 10^{13}$  vg ml<sup>-1</sup>)<sup>29</sup> and AAV<sub>2/9</sub>-fDIO-oChIEF-EGFP (titer of  $1.62 \times 10^{13}$  vg ml<sup>-1</sup>), into GPe with a volume ratio of 1:1, allowing expression of shRNA for Syt1 together with oChIEF/EGFP in a subpopulation of PV-Cre cells. A virus with nonspecific control (NC) shRNA (AAV<sub>2/8</sub>-DIO-mCherry-Flp-shRNA (NC) (titer of  $1.40 \times 10^{12}$  vg ml<sup>-1</sup>) was used together with the oChIEF/EGFP virus as a control.

To ablate GPe PV neurons, AAV<sub>2/9</sub>-CAG-DIO-taCaspase3-TEVP-WPRE-pA (titer of  $1.63 \times 10^{13}$  vg ml<sup>-1</sup>) was injected bilaterally into GPe of PV-Cre mice to allow specific expression of Caspase3 in GPe PV neurons, which would cause cell death 3–4 weeks after the virus injection. We carried out open field test and rotarod test before and 3–5 weeks after the virus injections. In some cases, the injection volume was reduced to 150–200 nl to prevent virus diffusion.

To optogenetically activate GPe axons projecting to the STN in rats, we unilaterally injected AAV2/8-hsyn-oChIEF-tdTomato ( $2.4 \times 10^{13}$  vg ml<sup>-1</sup>) into the GPe (coordinates from the bregma: AP -0.9 mm, ML -2.8 mm, DV -6.2 and 6.6 mm) to achieve non-specific expression of oChIEF in GPe neurons. All viruses mentioned above were purchased from Taitool or OBio, or BrainVTA.

### Implantation for behavior test

In experiments involving DBS, electrodes for electric stimulation were implanted into the STN on both sides (coordinates from the bregma: AP, -1.6 mm; ML,  $\pm 1.7$  mm; DV, -4.73 to -4.75 mm) in DD mice or those

with bilateral GPe PV neurons ablated. Bipolar DBS electrodes were fabricated from coated platinum-iridium wire with a diameter of 76.2  $\mu$ m (777000, A-M Systems). The electrodes were meticulously inspected to avoid short circuits before implantation.

For bilateral implantation of the guide cannula together with the DBS electrode, the electrode was attached and glued to the cannula (KD-MB-Fi, KeDouBC) with the electrode tip extending beyond the cannula by 500  $\mu$ m. Then, we implanted the cannula/electrode into the brain, making sure the electrode tip is located in the STN and the cannula -200  $\mu$ m above the STN.

In experiments with optic fiber implantation, optic fibers (200  $\mu$ m in diameter, Inper) were bilaterally implanted into the STN (coordinates from the bregma: AP -1.65 mm, ML  $\pm 1.7$  mm, DV -4.35 to -4.40 mm) of adult PV-Cre mice with dopamine depletion at least 4 weeks after virus injection. The optic fibers were positioned -300  $\mu$ m above the STN. Similar experiments were conducted in rats, but with optic fiber implantation into the ipsilateral STN (coordinates relative to the bregma: AP -3.7 mm, ML -2.7 mm, DV -7.45 to -7.50 mm).

For bilateral implantation of the optic fibers together with the DBS electrodes, the electrode was attached and glued to the optic fibers with the electrode tip extending beyond the optic fiber by 500  $\mu$ m. Then, we implanted the optic fibers/electrodes into the brain, making sure the electrode tip is located in the STN and the optic fiber -300  $\mu$ m above the STN.

In experiments aimed to reduce the AR strength through pharmacological manipulation, guide cannulas (KD-MB-Fi, KeDouBC) were implanted bilaterally into the brain and positioned -300  $\mu$ m above the STN on each side. Optic fibers or injection cannulas for drug delivery could be inserted separately as needed. After the surgeries, animals were allowed to recover for 4–6 days before behavior tests.

### Behavioral experiments

All behavioral assessments of mice were conducted in a square open field open field (35  $\times$  35 cm) equipped with a camera (C920 pro, Logitech) for real-time monitoring of mouse behavior from above. Before testing, mice were allowed to acclimate for at least 2 h on the same day. During the test, locomotion behaviors were videotaped, and the timing of stimulation was recorded. Movement analysis was performed using Deeplabcut (Version 2.2.3)<sup>63</sup>, Anymaze software (Version 7.4), and MATLAB (Version 2023a). We measured and compared the mean velocity, immobility time (80% sensitivity in Anymaze software), total immobility time, and total distance traveled in different experimental groups. In behavioral tests for rats, we used a larger open field (100  $\times$  100 cm), while all other experimental conditions remained similar to those of mice.

**DBS test.** The electric stimuli were delivered using a stimulus generator (STG4004-16MA; Multichannel Systems) and controlled by the corresponding software, MC Stimulus II (Version 3.5.11). We applied trains of bipolar pulses (each positive pulse followed immediately by a pulse of -10  $\mu$ A with the same total charge; Supplementary Fig. 1a). We delivered electric stimulation with current intensity ranging from 80  $\mu$ A to 140  $\mu$ A (with increment of 20  $\mu$ A) to determine the optimal stimulation current for each DD mouse, ensuring smooth movement without any aberrant activity. Each train of electric stimulation was administered for 1 min, either at 130 Hz or 20 Hz. Mean velocity before (Pre), during (Stim), and after (Post) the train stimulation was analyzed with a bin size of 60 s. There was an interval of at least 100 s between each stimulation train to allow recovery. These tests were conducted in both DD mice and PV cell-ablated mice. Mice were sacrificed for the examination of TH expression and verification of electrode or cannula positions.

**Bilateral drug administration with DBS test.** The DBS test was initially conducted as described above. Following this, a solution containing

bicuculline (BCC, 500  $\mu$ M) in normal ACSF or vehicle was delivered through the injection cannulas (KD-MB-Fi, KeDouBC; extending 600  $\mu$ m beyond the guide cannula) into the STN. A double-channel automatic injection pump (R462, RWD) was employed for simultaneous bilateral administration. 1  $\mu$ l liquid was administered locally to the STN at a rate of 100 nl/min. After the drug application, the injection cannula was left in the tissue for 5 min. The DBS test was repeated (using the same current intensity) ~20 min after the drug administration to assess the effect of BCC on DBS-induced behavior changes. To examine the injection sites and the diffusion of drugs, we injected cholera toxin subunit B (CTB) conjugated with Alexa Fluor 488 (CTB-488, 0.01% in ACSF) into the STN with the same volume of 1  $\mu$ l under experimental conditions similar to BCC administration.

**Open field optogenetics test.** Activation of axons was achieved by delivering pulsed blue light to the STN (1 ms in pulse width, 130 Hz or 20 Hz for 30 s, with a 90-s interval between each trial) using a LED (473 nm, PSU-H-FDA, Lasertack), 4–6 days after dopamine depletion. The power of the light was 4.7–5.5 mW at the tip of the optic fiber (continuous light). Each animal received 6 stimulation trains of 130 Hz or alternating frequencies (130/20 Hz and 130/45 Hz), with an inter-train interval of 7–10 min. For optogenetics testing of Syt1 knockdown and nonspecific control mice, alternating frequencies were utilized. The mean velocity before, during, and after the optic stimulation train was calculated with a bin size of 30 s.

**Bilateral optogenetic inhibition PV axons with STN DBS test.** In mice 4–6 days after dopamine depletion, we performed experiments with optogenetic inhibition of PV axons expressing eArch3.0. Optic inhibition was achieved by delivering continuous light beams to the STN (60 s in trial duration, 10 mW, 120-s interval between trials) using a LED (589 nm, PSU-H-FDA, Lasertack). The effects of electric DBS with and without optic inhibition on locomotion were monitored and compared.

**Bilateral drug administration with optic-DBS test.** Before drug administration, similar optic stimulation was applied to the STN in the open field using alternate frequencies (130 and 20 Hz). Paired optic fibers (extending 200  $\mu$ m beyond the guide cannula) were bilaterally inserted into the guide cannulas for these tests. For drug delivery, we inserted injection cannulas (extending 600  $\mu$ m beyond the guide cannula) bilaterally to the STN. A solution containing 1 mM EGTA-AM was then administered through the injection cannula. The volume of EGTA-AM administered was 500 nl on each side with an injection rate of 50 nl/min. As a strict control, an equal volume of vehicle was administered using the same experimental paradigm. Approximately 20 min after administration, the same optogenetic tests were repeated to evaluate the effect of EGTA-AM.

**Movement assessment of mice with PV neuron ablation.** To assess the impact of PV cell ablation on spontaneous movement in mice, we conducted the open field test and the rotarod test before and 3–4 weeks after the virus injection. Mice were acclimatized to the behavioral testing room for at least 15 min before each test. In the open field test, mice were gently placed in the center of the arena and their behavior was recorded for 10 min. Prior to each trial, the open field was thoroughly cleaned with 75% alcohol. For the rotarod test, we employed an apparatus set to accelerating mode (5–60 rpm, 10 min). The trial of test would be terminated if the mouse fell off the rod, and the latency to fall was automatically recorded by the apparatus. Each mouse was tested for two consecutive days, three trials per day with an interval of at least 10 min. The average latency of the three trials was calculated. Comparisons were made between the performance of individual mice before and after PV cell ablation to evaluate changes in motor function and motor learning ability.

## In vivo electrophysiological recordings

The recordings were conducted in awake, freely moving mice or rats using a custom-made 4-wire bundle of microelectrodes (RO 800, SANDVIK) with an impedance ranging from 1.5 to 2 M $\Omega$ . These electrodes were bound together with an optic fiber using a silica tube (TSP350450, Polymicro Technologies). Neuronal activity was sampled using the Zeus acquisition system (Bio-Signal Technologies), featuring 32 channels with a sampling rate of 30 kHz. Grounding was established to a screw positioned above the cerebellum, and online referencing was conducted against a wire implanted into the STN similar to recording electrodes. To isolate single-unit spikes, a Plexon Offline Sorter (Plexon Neuroscience Technologies, Dallas, TX, USA) was utilized. Common average referencing across all electrodes was implemented to mitigate motion artifacts arising from animal actions, such as head movement and grooming. Additionally, cross-channel artifacts appearing on at least 90% of channels were removed. Single-unit spike events across channels were detected and clustered using valley-seeking scanning for each experimental group. In experiments examining differences in LFP between DD rats and control rats, we recorded LFP for at least 30 min in each rat, and selected a stable segment of recording (10 min) for analysis.

## Immunohistochemistry

We performed TH immunostaining in DD animals. Animals were anesthetized with intraperitoneal injection of sodium pentobarbital (100 mg/kg of body weight) or Zoletil (50 mg/kg of body weight) and perfused transcardially with saline (0.9% NaCl), followed by 4% PFA. Brains were dissected out and post-fixed overnight in 4% PFA at 4 °C, then transferred to 30% sucrose. Coronal slices of bilateral striatum were cut using a cryostat microtome (CM1950, Leica) or a vibratome (VT-1200S, Leica) at a thickness of 40  $\mu$ m. Slices were mounted onto slides, rinsed in 0.01 M PBS three times (10 min each), permeabilized with 0.5% Triton X-100 for 30 min, and blocked with 5% BSA in PBS for 1 h. Following overnight incubation at 4 °C with the primary antibody (rabbit anti-TH, AB152, Millipore, 1:1000 in 0.1% Triton X-100), slides were washed again in 0.01 M PBS three times and incubated with the secondary antibody (Alexa Fluor 488 donkey anti-Rabbit, A-21206, Thermo, 1:1000 in 0.1% Triton X-100) for 2 h at room temperature. Confocal microscopy (Olympus, FV3000) with a 10x air objective was used to acquire images of the entire brain slices (z-stacks, 5  $\mu$ m per image).

In experiments involving PV cell ablation, we performed immunostaining using the PV antibody with a protocol similar to the TH staining. The primary and secondary antibodies were rabbit anti-PV (PV25, Swant, 1:500 in 0.1% Triton X-100) and Alexa Fluor-488 donkey anti-Rabbit (A-21206, Thermo, 1:1000 in 0.1% Triton X-100), respectively.

To examine the colocalization of mCherry and PV immunosignals in GPe neurons using the Cre-on and Cre-off system, we prepared 40- $\mu$ m-thick sagittal sections using a cryostat microtome (CM1950, Leica). The primary antibodies included rabbit anti-PV (PV25, Swant, 1:500 in 0.1% Triton X-100) and goat anti-mCherry (orb11618, Biorbyt, 1:500 in 0.1% Triton X-100), while the secondary antibodies were Alexa Fluor-488 donkey anti-Rabbit (A-21206, Thermo, 1:1000 in 0.1% Triton X-100) and Alexa Fluor-555 donkey anti-Goat (A21432, Thermo, 1:1000 in 0.1% Triton X-100). We obtained z-stack images (5  $\mu$ m per image) that were acquired using a 20x air objective and processed with ImageJ. Double-blind statistics were employed for data analysis.

## Statistics and reproducibility

Data analysis was performed using MATLAB and Spike2 software. All data in the text and figures were shown as mean  $\pm$  SEM. All measurements were taken from distinct samples. To quantify the synaptic responses induced by SR and AR, we first removed the electric artifacts from postsynaptic current traces induced by electric stimulation

(Supplementary Fig. 1b–d). This artifact-removing procedure was not required for the optic stimulation data. The total charge induced by the stimulation train is calculated as the total area under the curve of current trace. Because individual SR events are contaminated by AR events, we fit each SR event with an  $\alpha$ -synapse function ( $I(t) = g_{\max} \cdot \left(\frac{t - t_{\text{onset}}}{\tau}\right) \cdot e^{1 - \frac{t - t_{\text{onset}}}{\tau}}$ ,  $t > t_{\text{onset}}$ ) to estimate the SR charge (Supplementary Fig. 1c)<sup>64</sup>. Optimal fitting parameters, including  $\tau$  (the time to peak of the conductance),  $g_{\max}$  (the peak amplitude of the conductance), and  $t_{\text{onset}}$  (the time when conductance begins), were selected if a minimal difference between the fit and the raw trace was achieved. The charge of individual SR was quantified as the area under the fit curve. The total SR charge is the sum of all individual SR charge during the stimulation train. The AR charge is obtained by subtracting the SR charge from the total charge. The AR ratio is the ratio of AR charge to the total charge. The basal current induced by the train stimulation is DC shift of the current trace.

For in vivo single-unit recording data, we used Offline Sorter (Version 4.7.2) and NeuroExplorer (Version 5.438) to perform spike sorting and analysis of synchronicity between spikes, respectively. For each spike occurring at time  $t_n$  in a single unit, the inter-spike interval (ISI) was measured as  $(t_{n+1} - t_n)$ . For inter-cross-unit interval (ICUI) between paired units, we measured the interval between the reference spike at time  $t_n$  in one unit and the nearest spike in the other unit at time  $t_i$ , thus  $\text{ICUI} = \text{abs}(t_i - t_n)$  (see also Fig. 4h). The CV of ISI and ICUI were used for estimate the level of synchronization of spiking activities in STN neurons. For LFP analysis, we applied a low-pass filter (at 250 Hz) to the LFP data. All data were represented as the log of the power spectral density (PSD), followed by Z-score calculation for normalization. Beta oscillations were defined as neural activity within the range of 13–40 Hz, where 13–20 Hz and 20–40 Hz were considered as low and high beta, respectively.

Statistical analyses were performed using Prism (GraphPad Software, Version 9.5.0). Shapiro–Wilk test was first used for data normality test. Unpaired  $t$ -test or paired  $t$ -test was used if they were normally distributed, otherwise the Mann–Whitney  $U$ -test would be employed for unpaired data or non-parametric test (Wilcoxon matched-pairs signed rank test) for paired data. All statistical tests were two-sided. We used one-way or two-way ANOVA for comparison of multiple groups to examine the overall difference among groups, without post hoc pairwise comparisons and adjustments for multiple comparisons.

## Reporting summary

Further information on research design is available in the Nature Portfolio Reporting Summary linked to this article.

## Data availability

The data supporting the findings of this study are all available in the paper and related supplementary information files. Source data are provided with this paper. Big data files such as the Spike2 files of this study are available from the corresponding author (Y.S. yousheng@fudan.edu.cn) upon request. Source data are provided with this paper.

## Code availability

The codes used in this study are publicly available on GitHub: <https://github.com/ZongyiXu-a/STN-DBS-analysis>.

## References

- Deuschl, G. et al. A randomized trial of deep-brain stimulation for Parkinson's disease. *N. Engl. J. Med.* **355**, 896–908 (2006).
- Rodriguez-Oroz, M. C. et al. Bilateral deep brain stimulation in Parkinson's disease: a multicentre study with 4 years follow-up. *Brain* **128**, 2240–2249 (2005).
- Benabid, A. L., Chabardes, S., Mitrofanis, J. & Pollak, P. Deep brain stimulation of the subthalamic nucleus for the treatment of Parkinson's disease. *Lancet Neurol.* **8**, 67–81 (2009).
- Obeso, J. A. et al. Deep-brain stimulation of the subthalamic nucleus or the pars interna of the globus pallidus in Parkinson's disease. *N. Engl. J. Med.* **345**, 956–963 (2001).
- Koller, W. C., Lyons, K. E., Wilkinson, S. B., Troster, A. I. & Pahwa, R. Long-term safety and efficacy of unilateral deep brain stimulation of the thalamus in essential tremor. *Mov. Disord.* **16**, 464–468 (2001).
- Benabid, A. L. et al. Long-term suppression of tremor by chronic stimulation of the ventral intermediate thalamic nucleus. *Lancet* **337**, 403–406 (1991).
- Kupsch, A. et al. Pallidal deep-brain stimulation in primary generalized or segmental dystonia. *N. Engl. J. Med.* **355**, 1978–1990 (2006).
- Vidailhet, M. et al. Bilateral deep-brain stimulation of the globus pallidus in primary generalized dystonia. *N. Engl. J. Med.* **352**, 459–467 (2005).
- Vetkas, A. et al. Deep brain stimulation targets in epilepsy: Systematic review and meta-analysis of anterior and centromedian thalamic nuclei and hippocampus. *Epilepsia* **63**, 513–524 (2022).
- Johnson, K. A., Okun, M. S., Scangos, K. W., Mayberg, H. S. & de Hemptinne, C. Deep brain stimulation for refractory major depressive disorder: a comprehensive review. *Mol. Psychiatry*, <https://doi.org/10.1038/s41380-023-02394-4> (2024).
- Li, G. et al. Instantaneous antidepressant effect of lateral habenula deep brain stimulation in rats studied with functional MRI. *Elife* **12**, <https://doi.org/10.7554/eLife.84693> (2023).
- Bergman, H., Wichmann, T. & DeLong, M. R. Reversal of experimental parkinsonism by lesions of the subthalamic nucleus. *Science* **249**, 1436–1438 (1990).
- Filali, M., Hutchison, W. D., Palter, V. N., Lozano, A. M. & Dostrovsky, J. O. Stimulation-induced inhibition of neuronal firing in human subthalamic nucleus. *Exp. Brain Res.* **156**, 274–281 (2004).
- Moran, A., Stein, E., Tischler, H., Bebelovsky, K. & Bar-Gad, I. Dynamic stereotypic responses of Basal Ganglia neurons to subthalamic nucleus high-frequency stimulation in the parkinsonian primate. *Front. Syst. Neurosci.* **5**, 21 (2011).
- Tai, C. H. et al. Electrophysiological and metabolic evidence that high-frequency stimulation of the subthalamic nucleus bridges neuronal activity in the subthalamic nucleus and the substantia nigra reticulata. *Faseb J.* **17**, 1820–1830 (2003).
- Deng, S. et al. Regulation of recurrent inhibition by asynchronous glutamate release in neocortex. *Neuron* **105**, 522–533.e524 (2020).
- Jiang, M., Yang, M., Yin, L., Zhang, X. & Shu, Y. Developmental reduction of asynchronous GABA release from neocortical fast-spiking neurons. *Cereb. Cortex* **25**, 258–270 (2015).
- Manseau, F. et al. Desynchronization of neocortical networks by asynchronous release of GABA at autaptic and synaptic contacts from fast-spiking interneurons. *PLoS Biol.* **8**, <https://doi.org/10.1371/journal.pbio.1000492> (2010).
- Li, J., Deng, S., He, Q., Ke, W. & Shu, Y. Asynchronous glutamate release at autapses regulates spike reliability and precision in mouse neocortical pyramidal cells. *Cereb. Cortex* **31**, 2278–2290 (2021).
- Kühn, A. A. et al. High-frequency stimulation of the subthalamic nucleus suppresses oscillatory beta activity in patients with Parkinson's disease in parallel with improvement in motor performance. *J. Neurosci.* **28**, 6165–6173 (2008).
- Luo, F. & Südhof, T. C. Synaptotagmin-7-mediated asynchronous release boosts high-fidelity synchronous transmission at a central synapse. *Neuron* **94**, 826–839.e823 (2017).
- Ding, F. et al. Changes in the composition of brain interstitial ions control the sleep-wake cycle. *Science* **352**, 550–555 (2016).

23. Dong, J., Hawes, S., Wu, J., Le, W. & Cai, H. Connectivity and functionality of the globus pallidus externa under normal conditions and Parkinson's disease. *Front. Neural Circuits* **15**, 645287 (2021).
24. Mastro, K. J. et al. Cell-specific pallidal intervention induces long-lasting motor recovery in dopamine-depleted mice. *Nat. Neurosci.* **20**, 815–823 (2017).
25. Lilascharoen, V. et al. Divergent pallidal pathways underlying distinct Parkinsonian behavioral deficits. *Nat. Neurosci.* **24**, 504–515 (2021).
26. Jones, J. A., Higgs, M. H., Olivares, E., Peña, J. & Wilson, C. J. Spontaneous activity of the local GABAergic synaptic network causes irregular neuronal firing in the external globus pallidus. *J. Neurosci.* **43**, 1281–1297 (2023).
27. Ketzeff, M. & Silberberg, G. Differential synaptic input to external globus pallidus neuronal subpopulations in vivo. *Neuron* **109**, 516–529.e514 (2021).
28. Pan, M. K. et al. Neuronal firing patterns outweigh circuitry oscillations in Parkinsonian motor control. *J. Clin. Investig.* **126**, 4516–4526 (2016).
29. Bacaj, T. et al. Synaptotagmin-1 and synaptotagmin-7 trigger synchronous and asynchronous phases of neurotransmitter release. *Neuron* **80**, 947–959 (2013).
30. Hefft, S. & Jonas, P. Asynchronous GABA release generates long-lasting inhibition at a hippocampal interneuron-principal neuron synapse. *Nat. Neurosci.* **8**, 1319–1328 (2005).
31. Xu, W. et al. Distinct neuronal coding schemes in memory revealed by selective erasure of fast synchronous synaptic transmission. *Neuron* **73**, 990–1001 (2012).
32. Steiner, L. A. et al. Connectivity and dynamics underlying synaptic control of the subthalamic nucleus. *J. Neurosci.* **39**, 2470–2481 (2019).
33. Xiao, C. et al. Differential modulation of subthalamic projection neurons by short-term and long-term electrical stimulation in physiological and parkinsonian conditions. *Acta Pharmacol. Sin.* **43**, 1928–1939 (2022).
34. Gradinaru, V., Mogri, M., Thompson, K. R., Henderson, J. M. & Deisseroth, K. Optical deconstruction of Parkinsonian neural circuitry. *Science* **324**, 354–359 (2009).
35. Zhang, Y. et al. Targeting thalamic circuits rescues motor and mood deficits in PD mice. *Nature* **607**, 321–329 (2022).
36. Weiss, D. et al. Subthalamic stimulation modulates cortical motor network activity and synchronization in Parkinson's disease. *Brain* **138**, 679–693 (2015).
37. Whitmer, D. et al. High frequency deep brain stimulation attenuates subthalamic and cortical rhythms in Parkinson's disease. *Front. Hum. Neurosci.* **6**, 155 (2012).
38. Anderson, R. W., Farokhniaee, A., Gunalan, K., Howell, B. & McIntyre, C. C. Action potential initiation, propagation, and cortical invasion in the hyperdirect pathway during subthalamic deep brain stimulation. *Brain Stimul.* **11**, 1140–1150 (2018).
39. Li, S., Arbuthnott, G. W., Jutras, M. J., Goldberg, J. A. & Jaeger, D. Resonant antidromic cortical circuit activation as a consequence of high-frequency subthalamic deep-brain stimulation. *J. Neurophysiol.* **98**, 3525–3537 (2007).
40. Schor, J. S. et al. Therapeutic deep brain stimulation disrupts movement-related subthalamic nucleus activity in Parkinsonian mice. *Elife* **11**, <https://doi.org/10.7554/eLife.75253> (2022).
41. Valverde, S. et al. Deep brain stimulation-guided optogenetic rescue of Parkinsonian symptoms. *Nat. Commun.* **11**, 2388 (2020).
42. Milosevic, L. et al. A theoretical framework for the site-specific and frequency-dependent neuronal effects of deep brain stimulation. *Brain Stimul.* **14**, 807–821 (2021).
43. Remple, M. S. et al. Subthalamic nucleus neuronal firing rate increases with Parkinson's disease progression. *Mov. Disord.* **26**, 1657–1662 (2011).
44. Tai, C. H. Subthalamic burst firing: a pathophysiological target in Parkinson's disease. *Neurosci. Biobehav. Rev.* **132**, 410–419 (2022).
45. Zhang, H. et al. Sonic hedgehog mediates high frequency-dependent deep brain stimulation for the correction of motor deficits in a Parkinson's disease model. *Neurosci. Bull.* **40**, 1732–1738 (2024).
46. Levy, R. et al. Lidocaine and muscimol microinjections in subthalamic nucleus reverse Parkinsonian symptoms. *Brain* **124**, 2105–2118 (2001).
47. Heiss, J. D. et al. Convection-enhanced delivery of muscimol into the bilateral subthalamic nuclei of nonhuman primates. *Neurosurgery* **84**, E420–e429 (2019).
48. Yoon, H. H. et al. Optogenetic inactivation of the subthalamic nucleus improves forelimb akinesia in a rat model of Parkinson disease. *Neurosurgery* **74**, 533–540 (2014).
49. Yoon, H. H. et al. Optogenetic inhibition of the subthalamic nucleus reduces levodopa-induced dyskinesias in a rat model of Parkinson's disease. *Stereotact. Funct. Neurosurg.* **94**, 41–53 (2016).
50. Yu, C., Cassar, I. R., Sambangi, J. & Grill, W. M. Frequency-specific optogenetic deep brain stimulation of subthalamic nucleus improves parkinsonian motor behaviors. *J. Neurosci.* **40**, 4323–4334 (2020).
51. Cui, Q. et al. Dissociable roles of pallidal neuron subtypes in regulating motor patterns. *J. Neurosci.* **41**, 4036–4059 (2021).
52. Mastro, K. J., Bouchard, R. S., Holt, H. A. & Gittis, A. H. Transgenic mouse lines subdivide external segment of the globus pallidus (GPe) neurons and reveal distinct GPe output pathways. *J. Neurosci.* **34**, 2087–2099 (2014).
53. Hernández, V. M. et al. Parvalbumin+ Neurons and Npas1+ neurons are distinct neuron classes in the mouse external globus pallidus. *J. Neurosci.* **35**, 11830–11847 (2015).
54. Spix, T. A. et al. Population-specific neuromodulation prolongs therapeutic benefits of deep brain stimulation. *Science* **374**, 201–206 (2021).
55. Lin, J. Y., Lin, M. Z., Steinbach, P. & Tsien, R. Y. Characterization of engineered channelrhodopsin variants with improved properties and kinetics. *Biophys. J.* **96**, 1803–1814 (2009).
56. Mattis, J. et al. Principles for applying optogenetic tools derived from direct comparative analysis of microbial opsins. *Nat. Methods* **9**, 159–172 (2011).
57. Hass, C. A. & Glickfeld, L. L. High-fidelity optical excitation of cortico-cortical projections at physiological frequencies. *J. Neurophysiol.* **116**, 2056–2066 (2016).
58. Shu, Y., Yu, Y., Yang, J. & McCormick, D. A. Selective control of cortical axonal spikes by a slowly inactivating K<sup>+</sup> current. *Proc. Natl. Acad. Sci. USA* **104**, 11453–11458 (2007).
59. Shu, Y., Hasenstaub, A., Duque, A., Yu, Y. & McCormick, D. A. Modulation of intracortical synaptic potentials by presynaptic somatic membrane potential. *Nature* **441**, 761–765 (2006).
60. Wiest, C. et al. Local field potential activity dynamics in response to deep brain stimulation of the subthalamic nucleus in Parkinson's disease. *Neurobiol. Dis.* **143**, 105019 (2020).
61. Beurrier, C., Bioulac, B., Audin, J. & Hammond, C. High-frequency stimulation produces a transient blockade of voltage-gated currents in subthalamic neurons. *J. Neurophysiol.* **85**, 1351–1356 (2001).
62. Beurrier, C., Ben-Ari, Y. & Hammond, C. Preservation of the direct and indirect pathways in an in vitro preparation of the mouse basal ganglia. *Neuroscience* **140**, 77–86 (2006).
63. Mathis, A. et al. DeepLabCut: markerless pose estimation of user-defined body parts with deep learning. *Nat. Neurosci.* **21**, 1281–1289 (2018).
64. Yin, L. et al. Autapses enhance bursting and coincidence detection in neocortical pyramidal cells. *Nat. Commun.* **9**, 4890 (2018).

## Acknowledgements

This study was supported by National Natural Science Foundation of China (32130044 and T2241002, Y.S.), STI2030-Major Projects (2021ZD0202500, Y.S.), Program of Shanghai Academic/Technology Research Leader (21XD1400100, Y.S.), as well as Natural Science Foundation of Hunan (2025JJ40019, S.D.) and Changsha (kq2502169, S.D.).

## Author contributions

Y.S. conceived and designed the study. S.D. and Z.X. conducted preliminary exploration. Z.X. performed most of the experiments, with help from W.D. in extracellular recording in behaving mice and rats, W.D. and S.D. in behavioral tests, and S.Y. in virus injections and immunostaining experiments. Z.X. also conducted most of the data analysis, with help from S.D., W.D., S.Y., X.Z. C.Y., J.Y., J.W. J.L., and X.Z. performed the mouse breeding and genotyping. Z.X. and Y.S. wrote the manuscript, and all authors edited the paper.

## Competing interests

The authors declare no competing interests.

## Additional information

**Supplementary information** The online version contains supplementary material available at <https://doi.org/10.1038/s41467-025-59113-6>.

**Correspondence** and requests for materials should be addressed to Suixin Deng or Yousheng Shu.

**Peer review information** *Nature Communications* thanks Eric Lowet and the other, anonymous, reviewers for their contribution to the peer review of this work. A peer review file is available.

**Reprints and permissions information** is available at <http://www.nature.com/reprints>

**Publisher's note** Springer Nature remains neutral with regard to jurisdictional claims in published maps and institutional affiliations.

**Open Access** This article is licensed under a Creative Commons Attribution-NonCommercial-NoDerivatives 4.0 International License, which permits any non-commercial use, sharing, distribution and reproduction in any medium or format, as long as you give appropriate credit to the original author(s) and the source, provide a link to the Creative Commons licence, and indicate if you modified the licensed material. You do not have permission under this licence to share adapted material derived from this article or parts of it. The images or other third party material in this article are included in the article's Creative Commons licence, unless indicated otherwise in a credit line to the material. If material is not included in the article's Creative Commons licence and your intended use is not permitted by statutory regulation or exceeds the permitted use, you will need to obtain permission directly from the copyright holder. To view a copy of this licence, visit <http://creativecommons.org/licenses/by-nc-nd/4.0/>.

© The Author(s) 2025